NOAA Technical Memorandum ERL WPL-71

HF RADAR MEASUREMENTS OF SURFACE CURRENTS IN THE GERMAN BIGHT DURING MARSEN PHASE 2 PART I: 18 to 24 SEPTEMBER 1979

M. M. Janopaul
A. S. Frisch
R. S. Lyons

Wave Propagation Laboratory
Boulder, Colorado
May 1981

noaa NATIONAL OCEANIC AND ATMOSPHERIC ADMINISTRATION / Environmental Research Laboratories

NOAA Technical Memorandum ERL WPL-71

HF RADAR MEASUREMENTS OF SURFACE CURRENTS IN THE GERMAN BIGHT DURING MARSEN PHASE 2

PART I: 18 to 24 SEPTEMBER 1979

M. M. Janopaul
A. S. Frisch
R. S. Lyons

Wave Propagation Laboratory
Boulder, Colorado
May 1981

UNITED STATES
DEPARTMENT OF COMMERCE
Malcolm Baldrige,
Secretary

NATIONAL OCEANIC AND
ATMOSPHERIC ADMINISTRATION
James P. Walsh,
Acting Administrator

Environmental Research
Laboratories
Joseph O. Fletcher,
Acting Director

CONTENTS

HF RADAR MEASUREMENTS OF SURFACE CURRENTS IN THE GERMAN BIGHT DURING MARSEN PHASE 2
PART I: 18 to 24 SEPTEMBER 1979

M.M. Janopaul, A.S. Frisch, and R.S. Lyons
NOAA/ERL/Wave Propagation Laboratory
Boulder, Colorado 80303

ABSTRACT

Described is a field experiment in which surface currents were measured by HF radar (called CODAR) situated in the German Bight. This study is part of the large-scale, international effort, MARSEN. Presented herein are hourly maps of instantaneous surface currents, tidal-current ellipses, and direct current averages. Analysis of the surface flow identifies the principal local feature as cyclonic semidiurnal tidal currents. The dominant general feature of the surface flow is a relatively weak cyclic pattern. This is the first part of a serial presentation of the CODAR MARSEN data set.

1. INTRODUCTION

The NOAA Coastal Ocean Dynamics Applications Radar (CODAR) participated in the Marine Remote Sensing (MARSEN) Experiment, August to October 1979. The scientific objectives of MARSEN were to utilize wherever possible the complementary capabilities provided by remote sensing (active and passive) and conventional (in situ) techniques to investigate such scientific questions as the behavior of oceanic fronts; the generation of waves and currents by wind in finite-depth waters; and dynamics of short waves and their dependence on wind speed, currents, long waves, surface containment, etc., in relation to gaining detailed understanding of the processes by which imaging radars detect ocean surface phenomena. The scientific objectives of CODAR participation were to provide ground truth for the imaging

radar data, to refine and verify existing 3-D current-storm surge numerical models, and to correlate the response of the upper layers to storms and frontal systems.

The field operations of the MARSEN experiment were divided into two phases. The first phase was executed during 15 August 1979 to 15 September 1979 with emphasis on detecting oceanic fronts in the German Bight area. The second phase was executed 15 September 1979 to 15 October 1979 with emphasis on measuring waves, currents, and wind in the German Bight and Dutch offshore areas. CODAR data were taken during Phase 2.

During the whole year 1979, the Deutsches Hydrographisches Institut (DHI) conducted its own measuring program called "Jahr der Deutschen Bucht" ("Year of the German Bight"). This experiment, originally planned to be independent of MARSEN, was concentrated on systematic investigation of the current flow situation. These data, with CODAR data, will serve as a basis for checking and improving a 3-D baroclinic numerical model of the German Bight that is dynamically coupled to a 2-D North Sea model. Two current-meter locations lie within the CODAR coverage area, allowing comparison of flow at one location at the surface and at depth (Janopaul and Mittelstaedt, 1981).

2. TECHNIQUE DESCRIPTION

Measurement of ocean surface currents with high frequency (HF) radar is based on electromagnetic (EM) backscatter from waves having a wavelength one half that of the carrier (Crombie, 1955). Although all wavetrains interact with a ground-wave mode radar, which virtually "floods" the sea surface, the only two that can backscatter energy toward the radar are those two that have wavelengths equal to half the radar wavelength, i.e., the trains moving toward and away from the radar (Barrick, 1978). HF radar surface-current measurements, like current-meter (CM) measurements, are representative of the total current, i.e., the interactive sum of geostrophic, tidal, wave, and wind generated components.

The CODAR system can produce detailed, synoptic surface-current measurements for an area on the order of 10^3 km^2 (Barrick et al., 1977). Analyses show HF radar senses the mean current to a depth of approximately the radar wavelength

divided by 8π from the (average) surface level (Barrick et al., 1974; Stewart and Joy, 1974); when transmitting at the standard frequency of 25.4 MHz, CODAR measures current velocity within a layer one-half meter from the (average) sea surface level. This frequency also dictates that the EM backscatter is from 6-m waves, and any Fourier decomposition of a given sea surface area always contains energy at or near the 6-m wavelength (Barrick, 1978). During studies of surface-current resolution, independent drifter-buoys showed HF radar accuracy to be better than 10 cm/s (Barrick et al., 1974; Stewart and Joy, 1974); when a 16-μs pulse width is used, which is equivalent to a 2.4 km length, the accuracy of CODAR measurements can be expected to be within this 10 cm/s range (Frisch and Weber, 1980).

3. EXPERIMENT

The radars were situated in the German Bight on Helgoland (54° 11.25' N, 7° 52.25' E) and at St. Peter-Ording (54° 19.75' N, 8° 35.20' E), 49 km apart (Fig. 1). The receiver boresight on Helgoland was 42° true north (TN), and the one at St. Peter-Ording was 282° TN. Transmissions went north and east from Helgoland and north and west from St. Peter-Ording. The common coverage area, on the order of 4000 km^2, was between the two sites and from about 54° 00' N to about 54° 40' N.

The planned CODAR sampling schedule was an observation, a period of 36 minutes, every 4 h on a 24 h basis from 17 September to 12 October 1979, and hourly during overflights. However, because of the heavy radio interference experienced, especially from 0800 to 1600 on Helgoland, the sampling rate was increased to hourly on Helgoland during 24 September 1979 and at St. Peter-Ording on 1 October 1979. Actual periods of observation for 17 to 24 September 1979 are shown in Table 1.

A wind recorder on Helgoland sampled hourly. Its record shows that there were strong westerly winds until 22 September. From noon 22 September to noon 23 September northerly winds prevailed, with a shift to southerly until early 24 September. Observations of meteorological conditions at St. Peter-Ording noted the same wind velocities. Both locations remarked upon the strongest winds and highest tides during 21 September.

4. DATA REDUCTION AND PRESENTATION

Data were numerically edited in three steps: (i) a standard deviation, s, was calculated from the current vectors within a 78.5 km^2 area (5.0 km radius) about a given location; (ii) Vectors more than 1.0 s from the mean were not included in any further calculations; and (iii) a mean vector for that area was calculated from those data within 1.0 s of the mean.

The known accuracy range of CODAR, 10 cm/s or better, applies to that area between the two sites and between 5 and 45 km north of the baseline (i.e., the line joining the sites). The returning echo from this northern coverage area had a signal-to-noise ratio (S/N) on the order of 10^3 to 10^6. The area of similar dimensions south of the baseline (i.e., the southern coverage area) gave a much weaker return, having a S/N on the order of 10^0 to 10^3. The majority of this difference in return was a result of (i) the directionality of the transmitting antennas, and (ii) greater path loss incurred because of longer distances over land between the antennas and the sea.

The radial component of velocity is not resolvable in an area near the baseline (Barrick et al., 1977). For MARSEN, this area was about 5 km on both sides of the baseline near each site, increasing to about 25 km at the center of the baseline (i.e., about half the total baseline length; personal communication, J.A. Leise, NOAA/ERL/WPL). Velocities in this elliptical area were computed from an interpolation program developed by J.A. Leise. The entire data set including the baseline area is edited statistically by globally removing data exceeding 2.5 s from the mean; this was done separately for the east, u, and north, v, velocity components. The removed data were estimated by means of a local algorithm which adds points to the periphery of those data within 2.5 s of the mean; this is a recursive replacement of a missing value with the average of the immediate neighbor values.

Instantaneous surface currents are presented (Fig. 2 to 38) for 0-, 4-, 8-, 12-, 16-, and 20-h observations from 0000 18 September to 0000 24 September. These vector maps represent a 4000 km^2 area as a (10 x 10) km^2 grid oriented parallel to the baseline. If fewer than 400 vectors (10 parallel to the baseline x 20 perpendicular to the baseline) appear on any one map, the missing vectors are in areas with returns having a S/N of less than 10^3.

Tidal currents for this period (Fig. 39) are computed (by the least-square method) estimates of the nominal 12-h tidal components for the surface currents as a function of position (Frisch and Weber, 1980). Component analysis of these tidal ellipses (Fig. 41 to 42) separates velocity into a north, u, and a west, v, component; each figure follows the change of a component with time and with latitude along a line of longitude. A baseline model (Lyons and Frisch, 1980), using a simulation of the MARSEN data set, showed that data for 2 days are necessary to obtain less than 20% error for recovery of a nominal 12-h component, but 6 days are necessary to recover the 12.00 and 12.42 components to this accuracy.

Mean currents (Fig. 43 to 48) were computed for each of the six 24-h periods, from 0018 (the center of the 0000 observation) to 0018 the following day. These values are composites of the mean wind-driven circulation, tidal-driven residuals, and other low-frequency (less than 24-h) forcing such as density driven currents, etc.

5. DISCUSSION

Because processing is very time consuming (every minute of field data took 4 minutes of computer time) we have decided to make the data available, especially to our MARSEN co-investigators, as soon as they are processed, rather than providing no results until the entire set is processed. Each release will include the instantaneous vector maps of only the newly processed data, but tidal analysis for all processed data. We will not present an in-depth analysis in any but the last set, and simply point out the major features of surface flow in prior sets.

The instantaneous currents are obviously dominated by the semidiurnal tides; the majority of the tidal ellipses are cyclic. This agrees with a general cyclic flow described for the entire German Bight in earlier studies (Böhnecke, 1922; Lee and Ramster, 1976). A finer scale study (Goedecke, 1968) identifies a system of cyclic eddy features extending northwest from the Elbe. The removal of the nominal semidiurnal tides (Fig. 44 to 48) shows that the direct current is relatively weak.

Review of all the data is serving as a developmental tool for CODAR. Our hardware, software, and field operations have benefitted from MARSEN with improvements in determining accuracy, methods of calculation, and sampling schemes.

One should keep in mind that maps presented here and in future reports are areal and temporal averages. Direct comparison of a CODAR vector with a conventional vector from a point measurement for the same location may be questionable. Each CODAR data point in this report represents the mean over a 78.5 km^2 area and over 36 min. Beyond this consideration, comparisons with current meter data should examine vertical shear, particularly in shallow areas subject to bottom friction.

6. ACKNOWLEDGMENTS

This research was supported by the Office of Naval Research and by Ocean Technology and Engineering Services, NOAA. The NOAA Sea State Studies field crew did an outstanding job in all phases of their work. The cooperation and assistance of Max Plank Institute for Meteorology and University of Hamburg personnel, especially H. Essen and F. Schirmer, are especially appreciated.

7. REFERENCES

Barrick, D.E., 1978: HF radio oceanography - A review, Boundary-Layer Meteorology, 23-43.

Barrick, D.E., J.M., Headrick, R.W. Bogle, and D.D. Crombie, 1974: Sea backscatter at HF: Interpretation and utilization of the echo, Proc. IEEE 62, 673-680.

Barrick, D.E., M.W. Evans, and B.L. Weber, 1977: Ocean surface currents mapped by radar, Science, 138-144.

Böhnecke, G., 1922: Salzegehalt und Strömungen der Nordsee, Veröff. Inst. Meeresk. Univ. Berlin, N.F.A. 10:1 34.

Crombie, D.D., 1955: Doppler spectrum of sea echo at -13.56 Mc/s, Nature 175, 681-682.

Frisch, A.S., and B.L. Weber, 1980: A new technique for measuring tidal currents by using a two-site HF Doppler radar system, J. Geophys. Res., 85, 3, 485-493.

Goedecke, E., 1968, Über die hydrographische Struktur der Deutschen Bucht im Hinblick auf die Verschmutzung in der Konvergenzzone. Helgol. Wiss. Meeresunters., 17: 108-125.

Janopaul, M.M., and E. Mittelstaedt, 1981: Comparison of remote HF radar current measurements with conventional data (submitted to J. Phys. Oceanogr.).

Lee, A.J., and J.W. Ramster, 1976, Atlas of the seas around the British Isles. Fish. Res. Tech. Rep., MAFF Direct. Fish. Res. Lowestoft, 20, 4 pp.

Lyons, R.S., and A.S. Frisch, 1980: Simulations of surface tidal current calculations for HF radar applications, NOAA Technical Memorandum ERL WPL-61.

Stewart, R.H., and J.W. Joy, 1974: HF radio measurements of surface currents, Deep Sea Res., 21, 1039-1049.

Table 1.--MARSEN 1979 Phase 2 CODAR Observations 17 to 24 September

	Helgoland (54° 11.25' N, 7° 52.25' E)	St. Peter-Ording (54° 19.75' N, 8° 35.20' E)
	From/To	From/To
17 September*	2002/2045	2005/2050
18 September	0000/0036	0000/0036
	0400/0436	0400/0436
	0800/0836	0800/0836
	1200/1236	1200/1236
	1602/1638	1600/1636
	2000/2036	2000/2036
19 September	0000/0036	0000/0036
	0400/0436	0400/0436
	0800/0836	0800/0836
	1200/1236	1200/1236
	1600/1636	1600/1636
	2000/2036	2000/2036
20 September	0000/0036	0000/0036
	0400/0436	0401/0437
	0803/0839	0801/0837
	1200/1236	1200/1236
	1601/1637	1600/1636
	2000/2036	2000/2036
21 September	0000/0036	0000/0036
	0535/0636	0400/0436
	0800/0836	0800/0836
	1200/1236	1200/1236
	1300/1336	1300/1336
	1600/1636	1600/1636
	2000/2036	2000/2036
22 September	0000/0036	0000/0036
	0400/0436	0400/0436
	0800/0836	0800/0836
	1000/1036	1000/1036
	1100/1136	1100/1136
	1200/1236	1200/1236
	1300/1336	1300/1336
	1400/1436	1400/1436
	1500/1536	1500/1536
	1600/1636	1600/1636
	1700/1736	1700/1736
	1800/1836	1800/1836
	1900/1936	1905/1941
	2000/2036	2000/2036
23 September	0000/0036	0000/0036
	0400/0436	0400/0436
	0800/0836	0800/0836
	1200/1236	1200/1236
	1600/1636	1600/1636
	2000/2036	2000/2036
24 September	0000/0036	0000/0036

* (all times given are in LT, GMT+1)

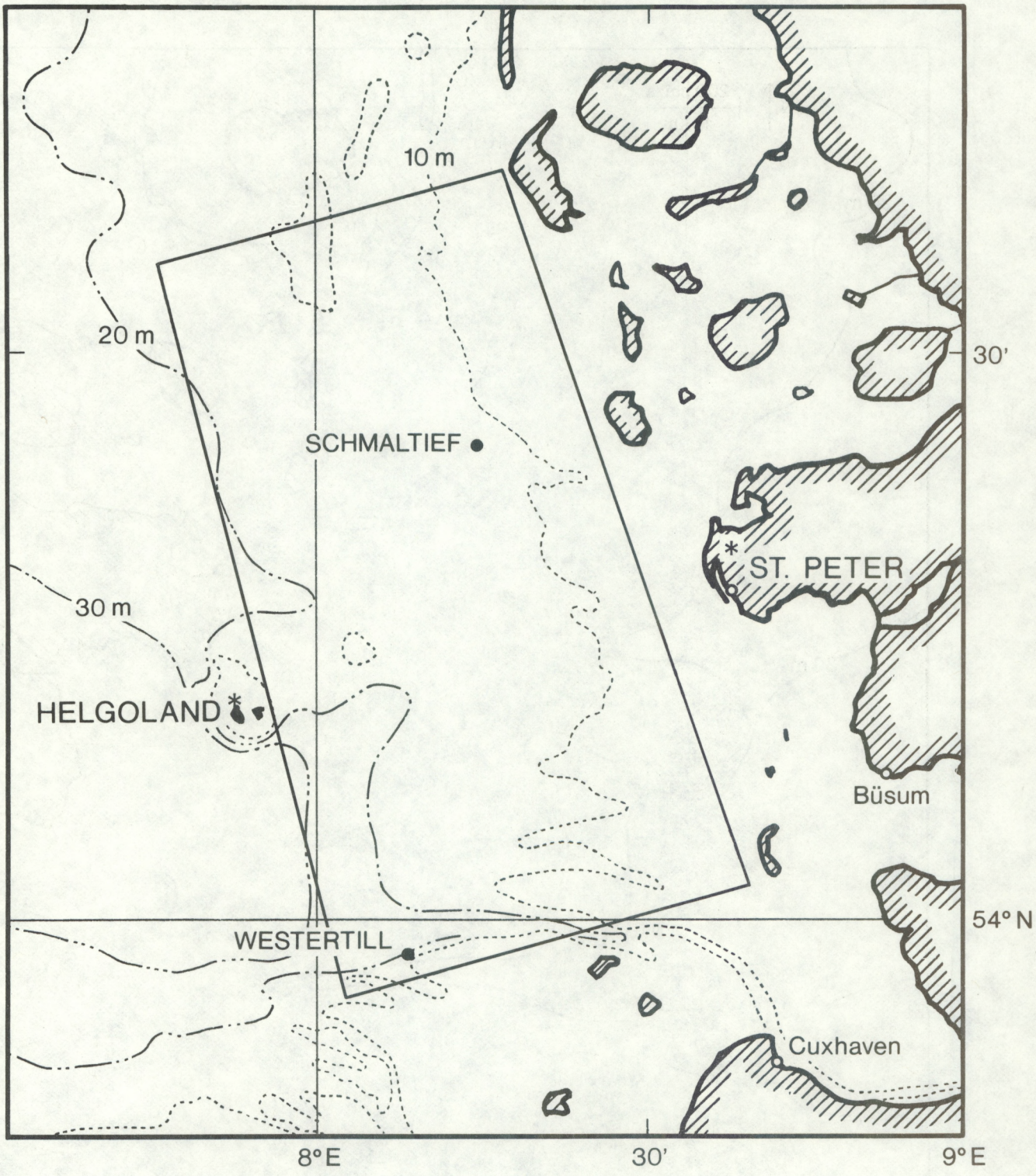

Figure 1.--Locations of CODAR sites in German Bight: Helgoland (54° 11.25' N, 7° 52.25'E) and St. Peter-Ording (54° 19.75' N, 8° 35.20'E). The CODAR coverage area (box) was on the order of 4000 km^2. Current meters in the CODAR coverage area were deployed at SCHMALTIEF (7 m: 54° 25.00' N, 8° 14.90'E) and WESTERTILL (11 and 25 m: 53° 58' N, 8° 7.00' E).

Figure 2.--Instantaneous surface current vectors 0000 18 September 1979.

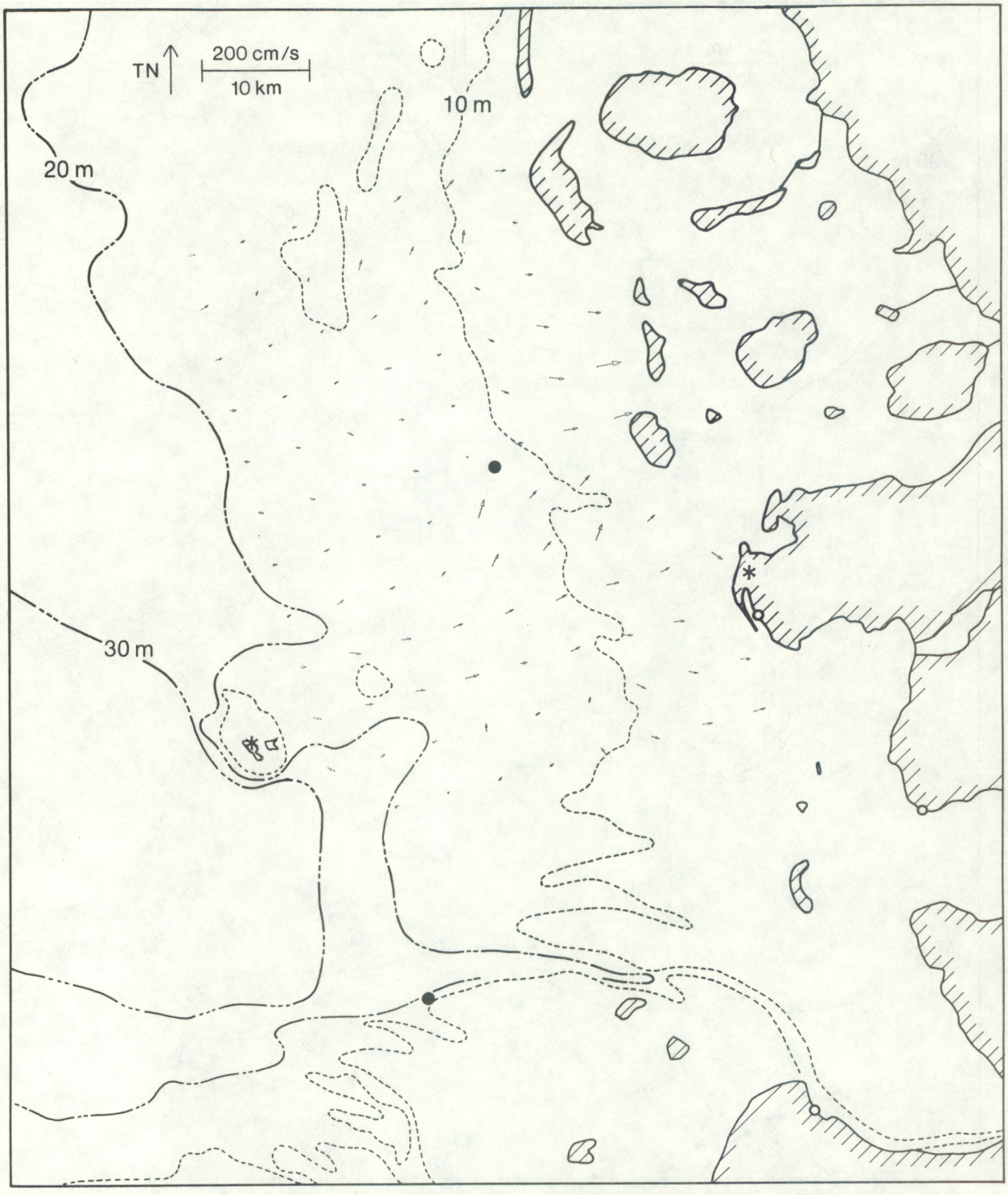

Figure 3.--Instantaneous surface current vectors 0400 18 September 1979.

Figure 4.--Instantaneous surface current vectors 0800 18 September 1979.

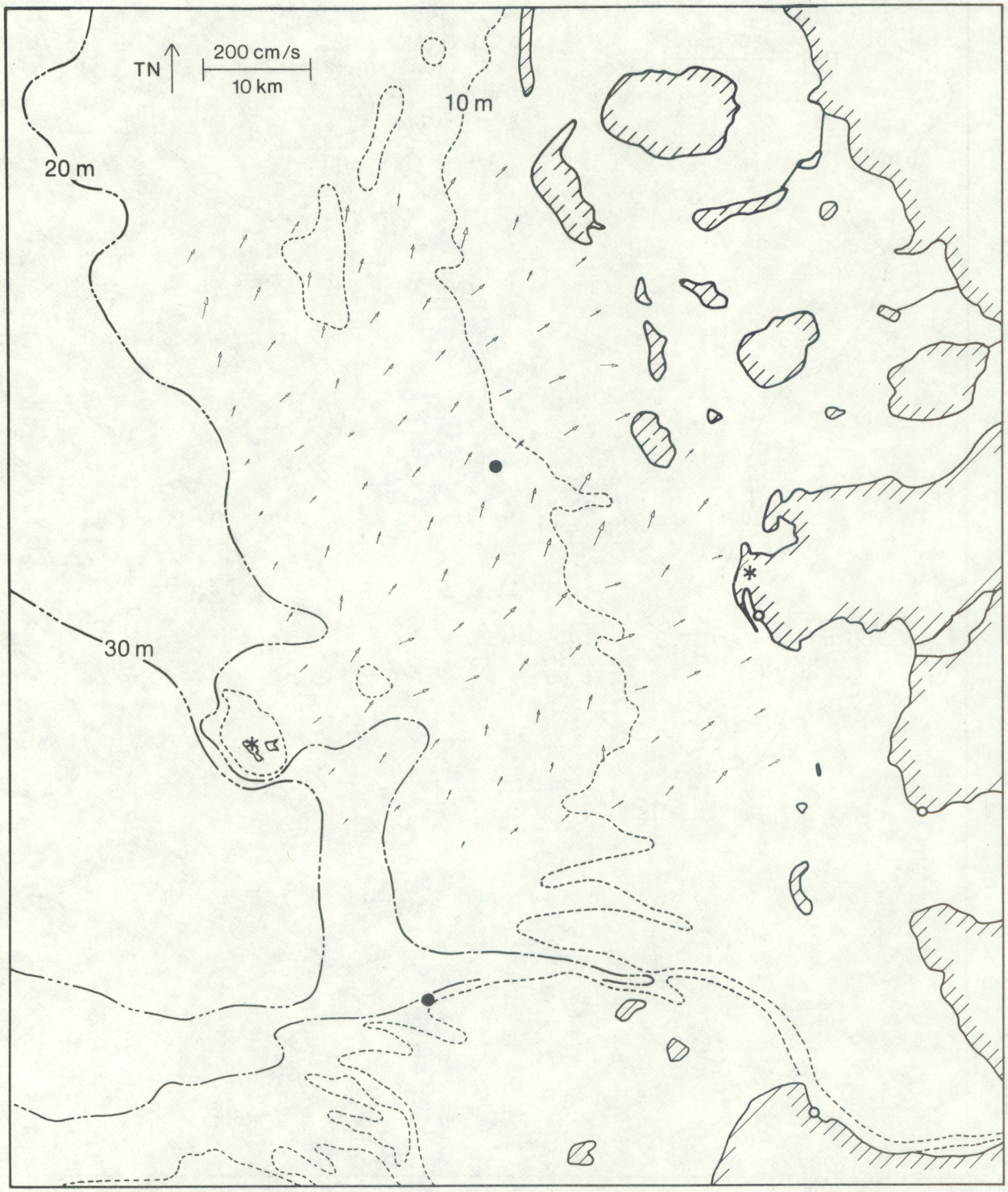

Figure 5.--Instantaneous surface current vectors 1200 18 September 1979.

Figure 6.--Instantaneous surface current vectors 1600 18 September 1979.

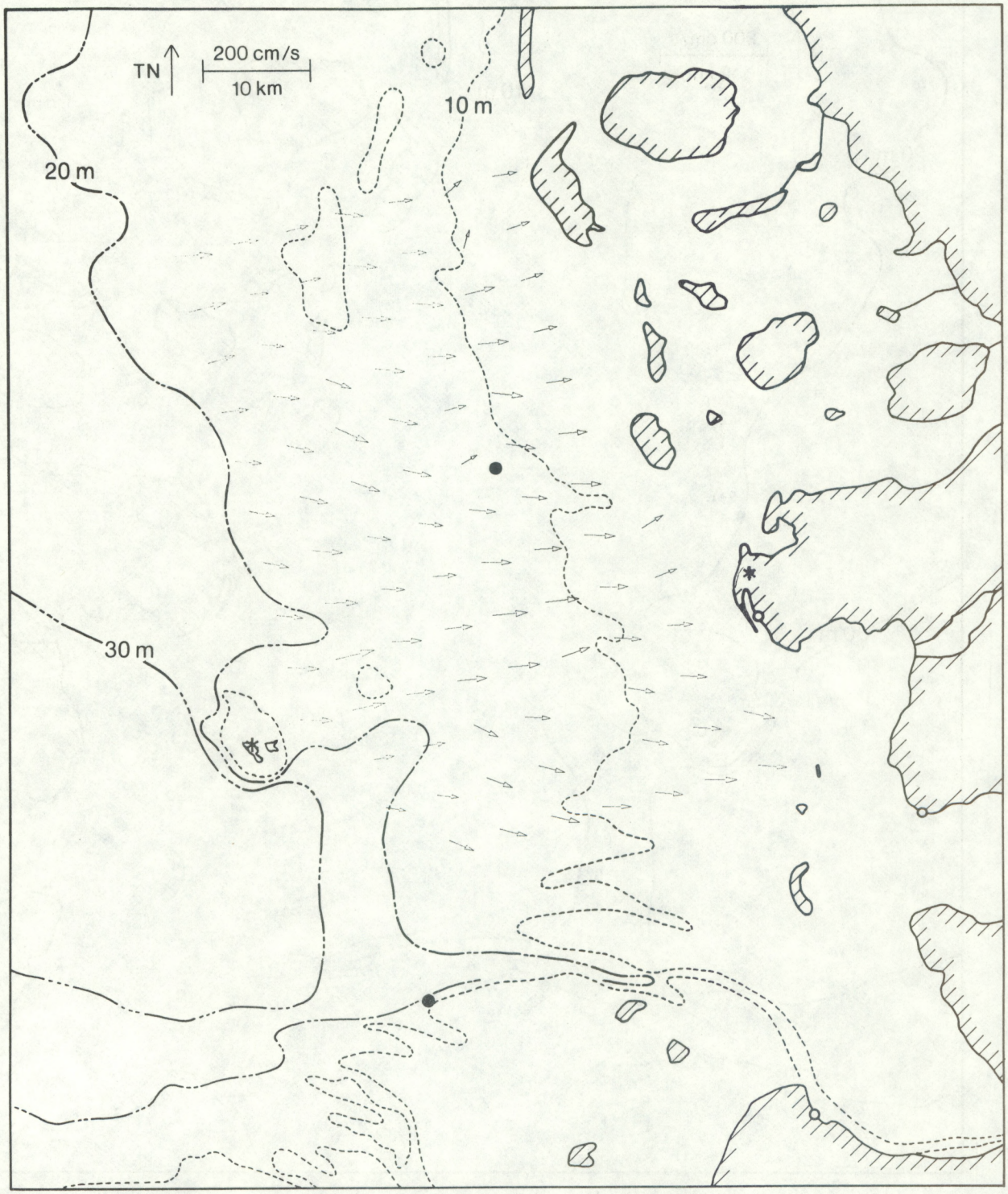

Figure 7.--Instantaneous surface current vectors 2000 18 September 1979.

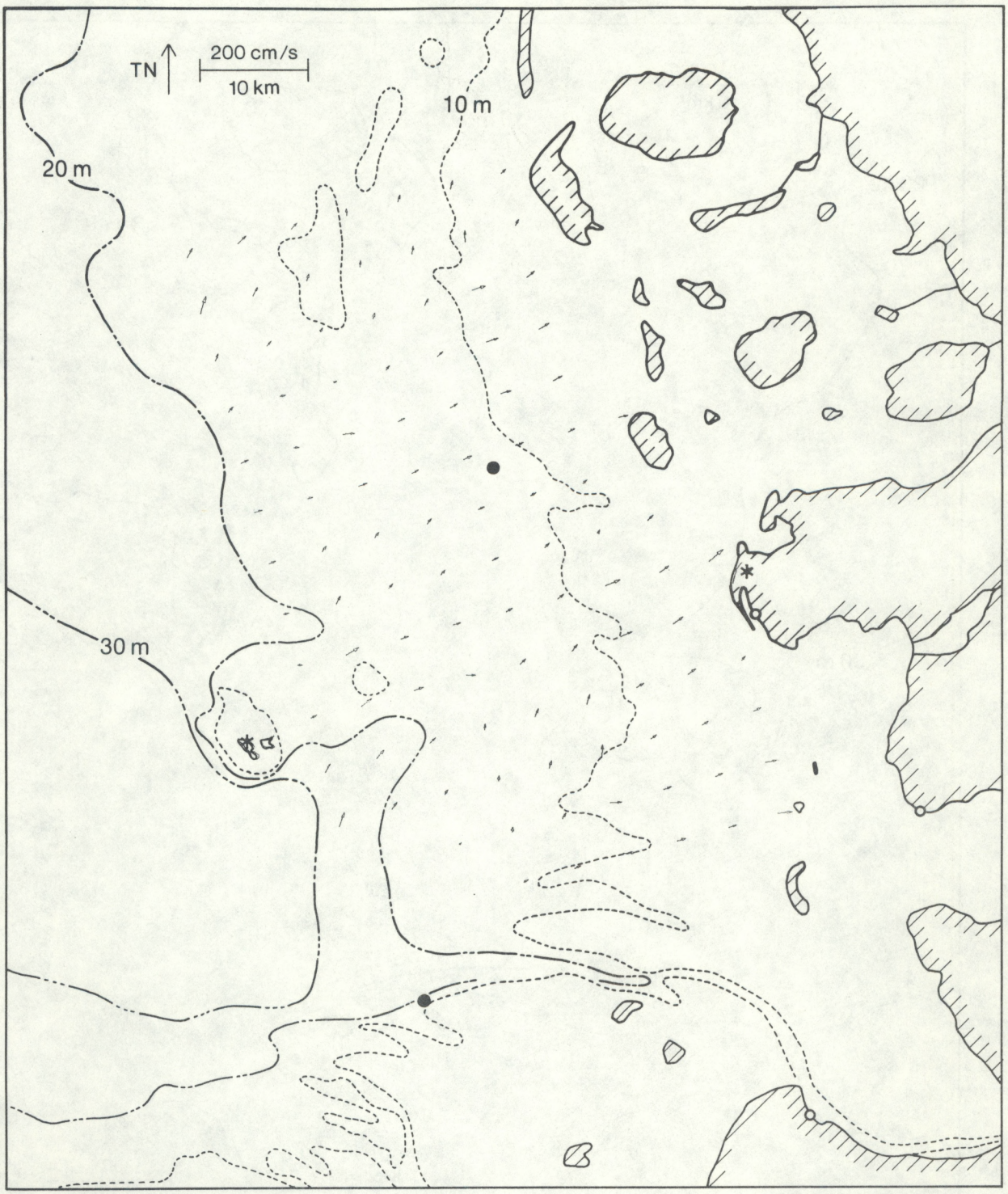

Figure 8.--Instantaneous surface current vectors 0000 19 September 1979.

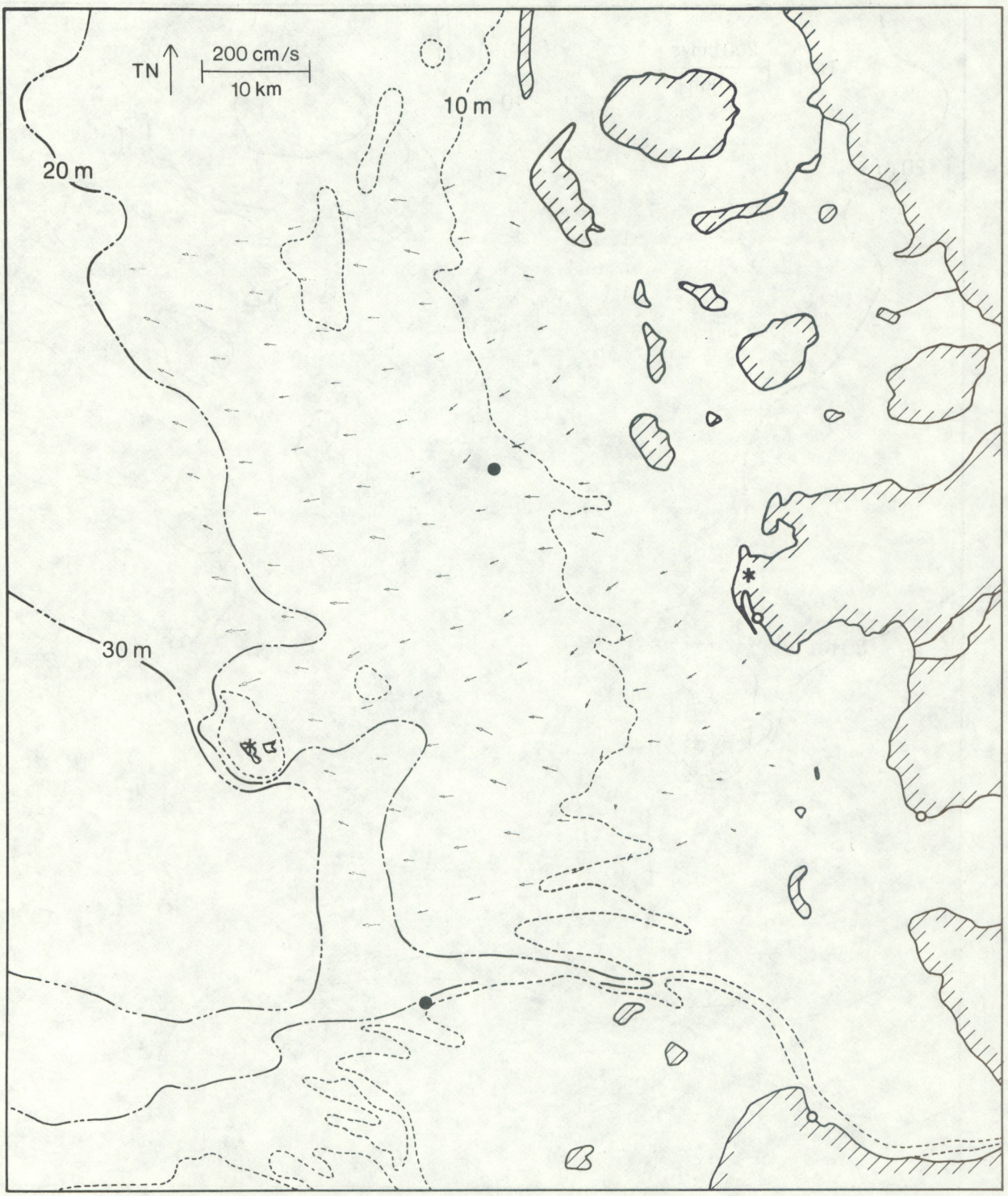

Figure 9.--Instantaneous surface current vectors 0400 19 September 1979.

Figure 10.--Instantaneous surface current vectors 0800 19 September 1979.

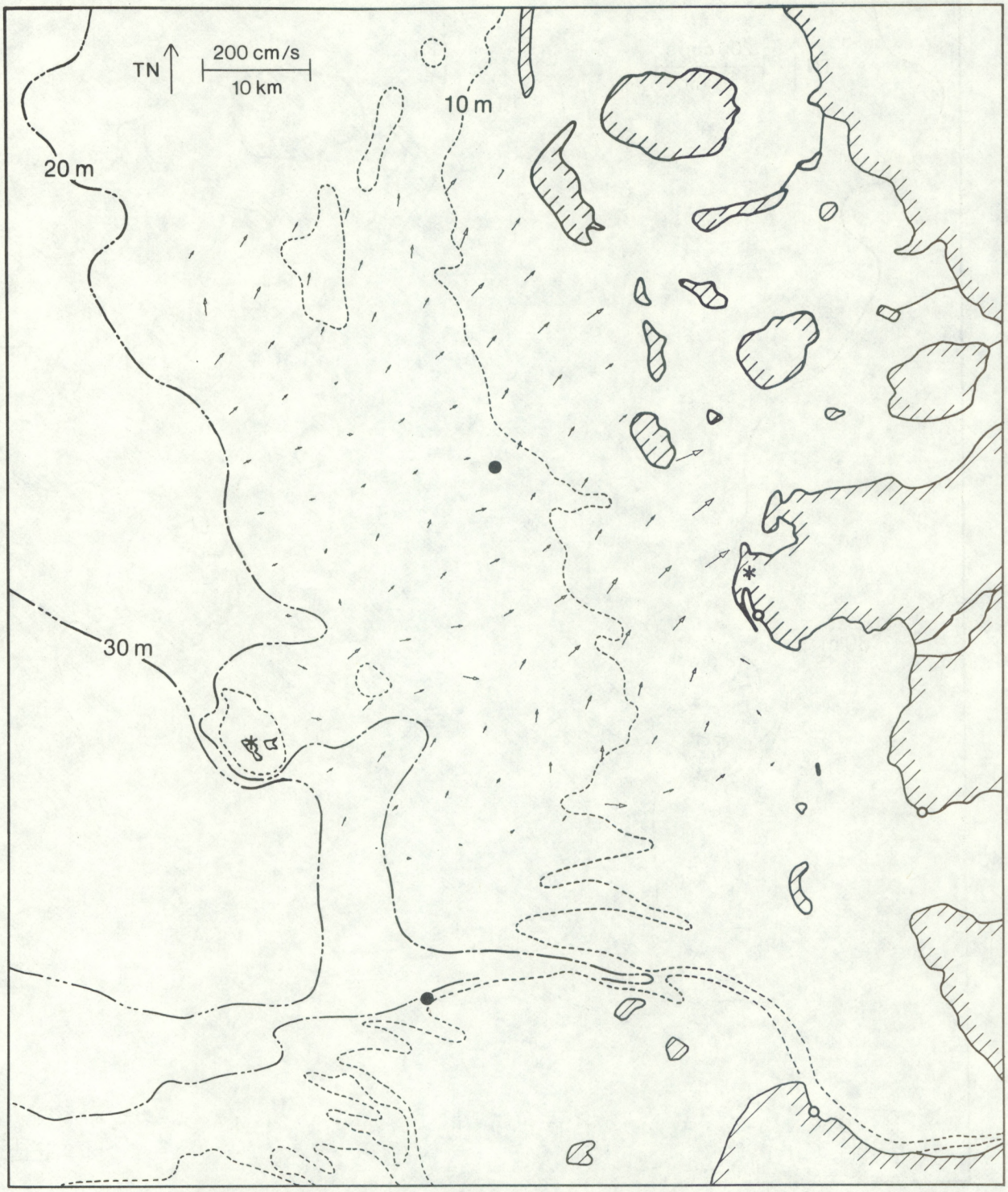

Figure 11.--Instantaneous surface current vectors 1200 19 September 1979.

Figure 12.--Instantaneous surface current vectors 1600 19 September 1979.

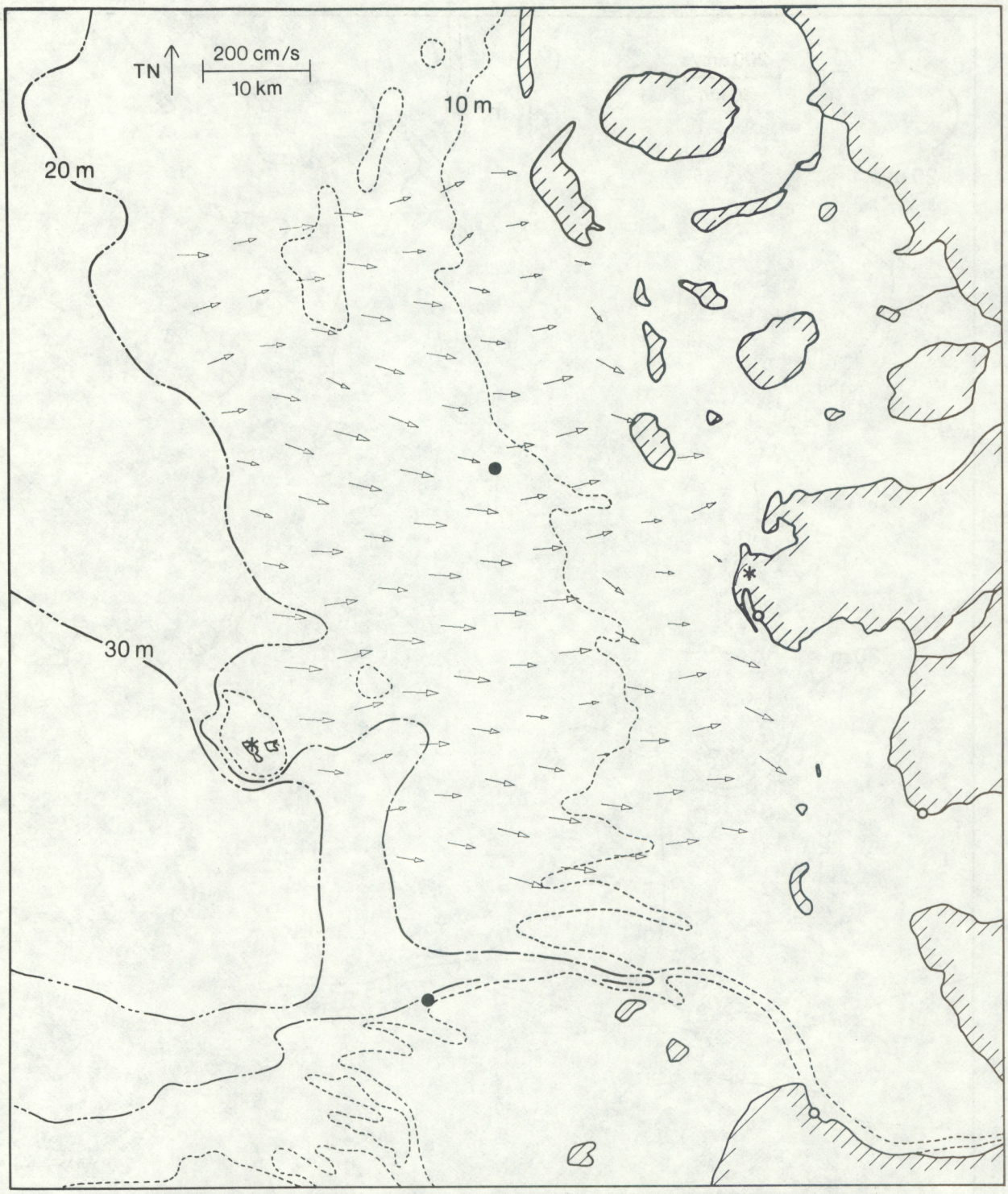

Figure 13.--Instantaneous surface current vectors 2000 19 September 1979.

Figure 14.--Instantaneous surface current vectors 0000 20 September 1979.

Figure 15.--Instantaneous surface current vectors 0400 20 September 1979.

Figure 16.--Instantaneous surface current vectors 0800 20 September 1979.

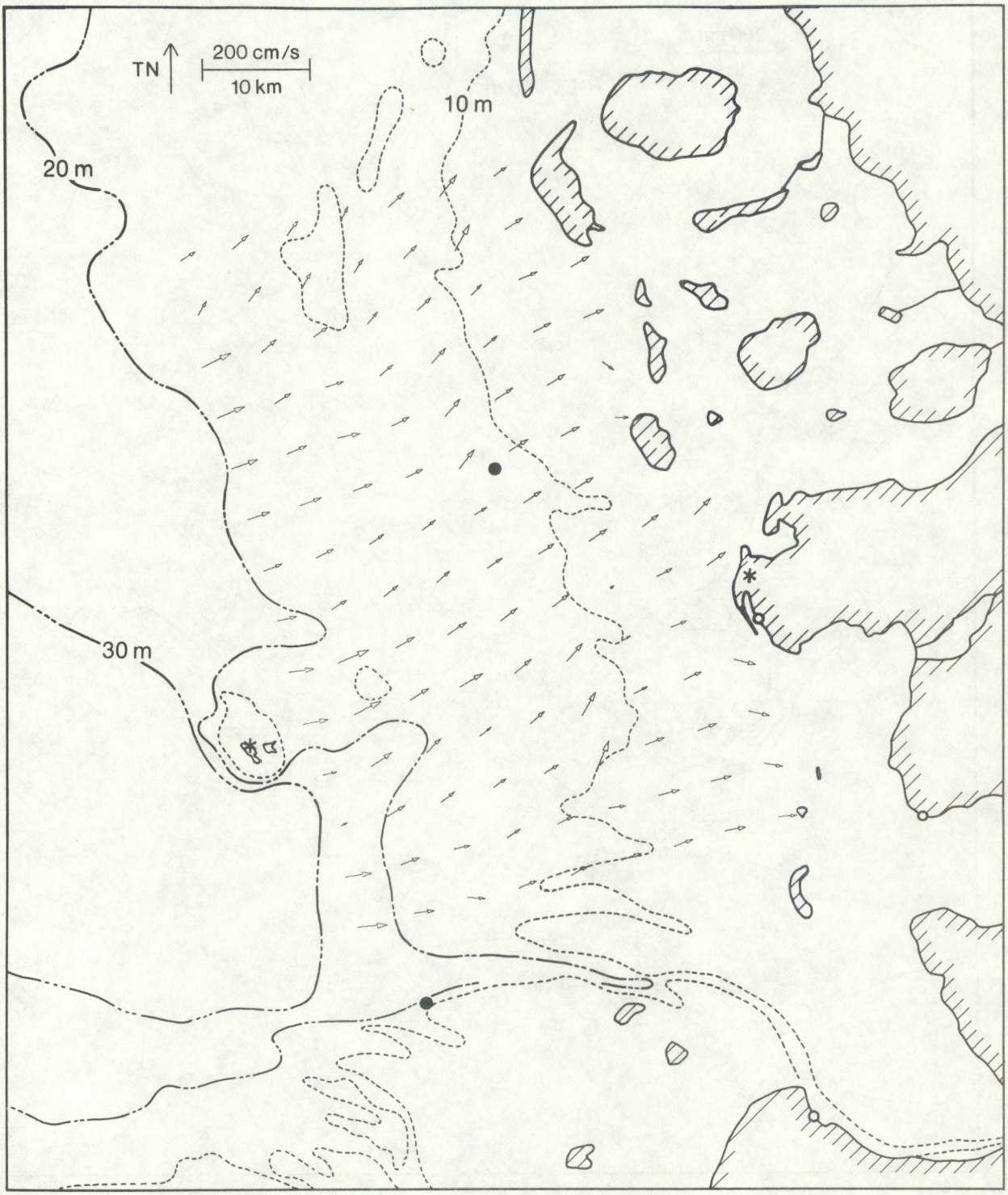

Figure 17.--Instantaneous surface current vectors 1200 20 September 1979.

Figure 18.--Instantaneous surface current vectors 1600 20 September 1979.

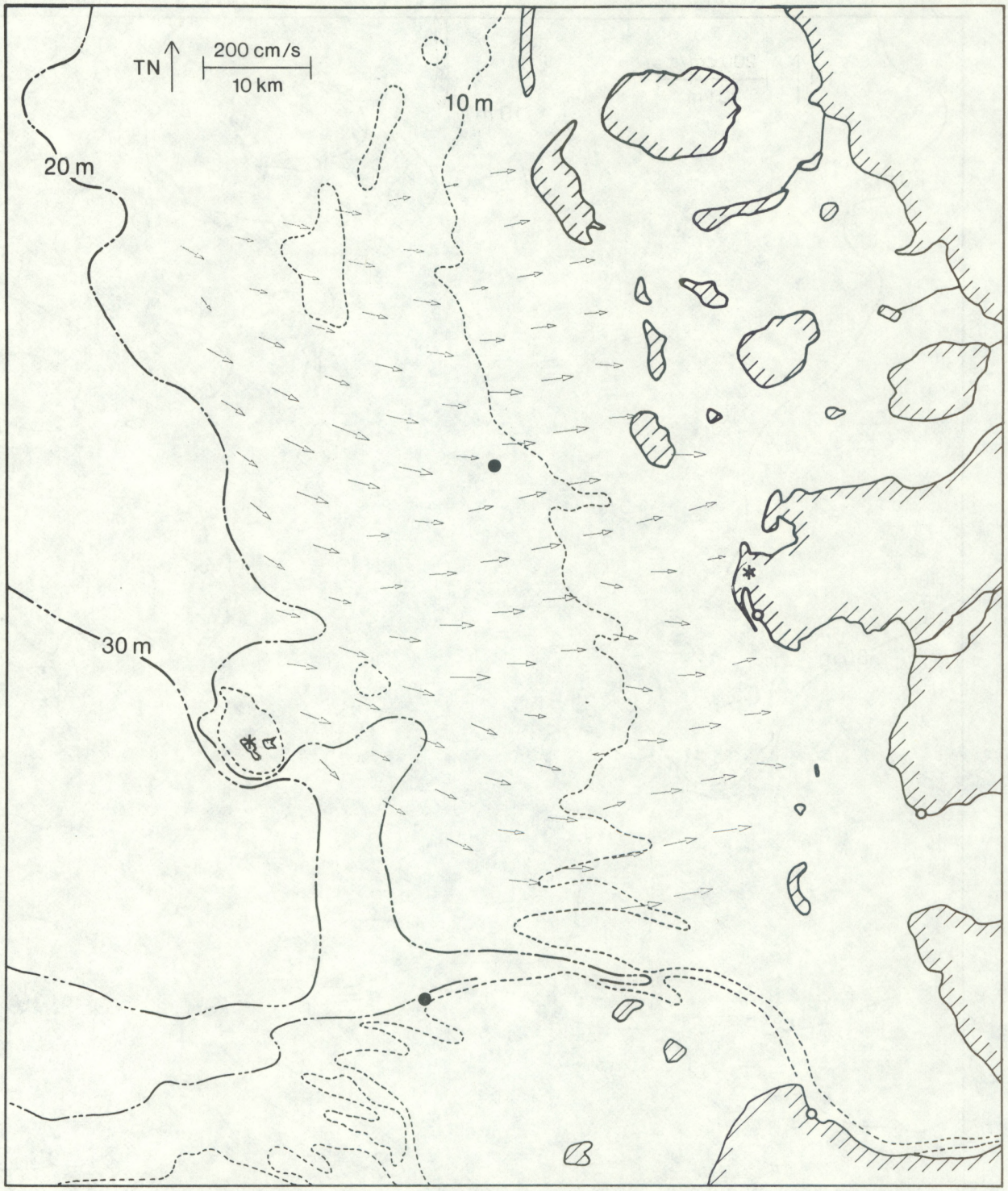

Figure 19.--Instantaneous surface current vectors 2000 20 September 1979.

Figure 20.--Instantaneous surface current vectors 0000 21 September 1979.

Figure 21.--Instantaneous surface current vectors 0400 21 September 1979.

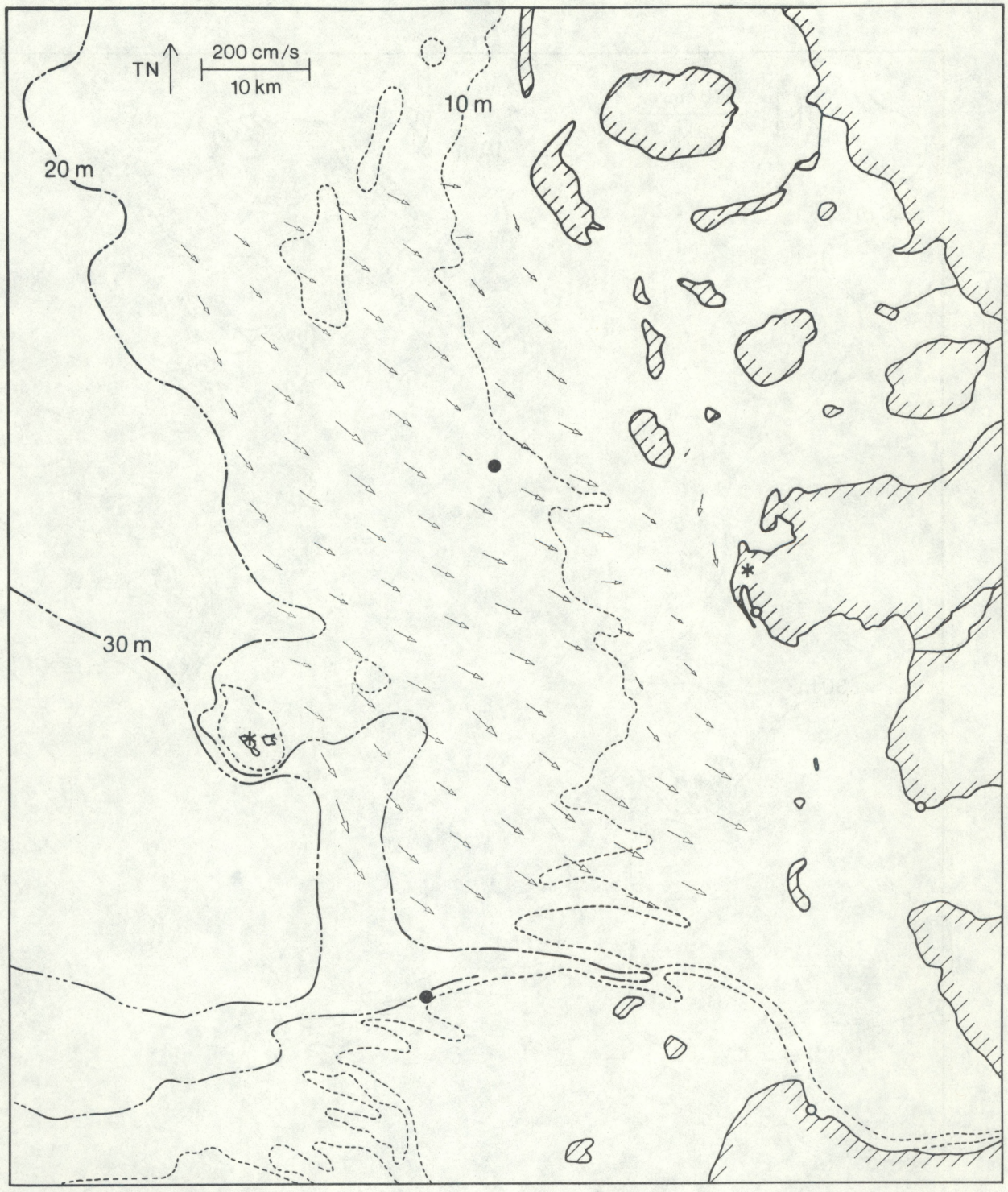

Figure 22.--Instantaneous surface current vectors 0800 21 September 1979.

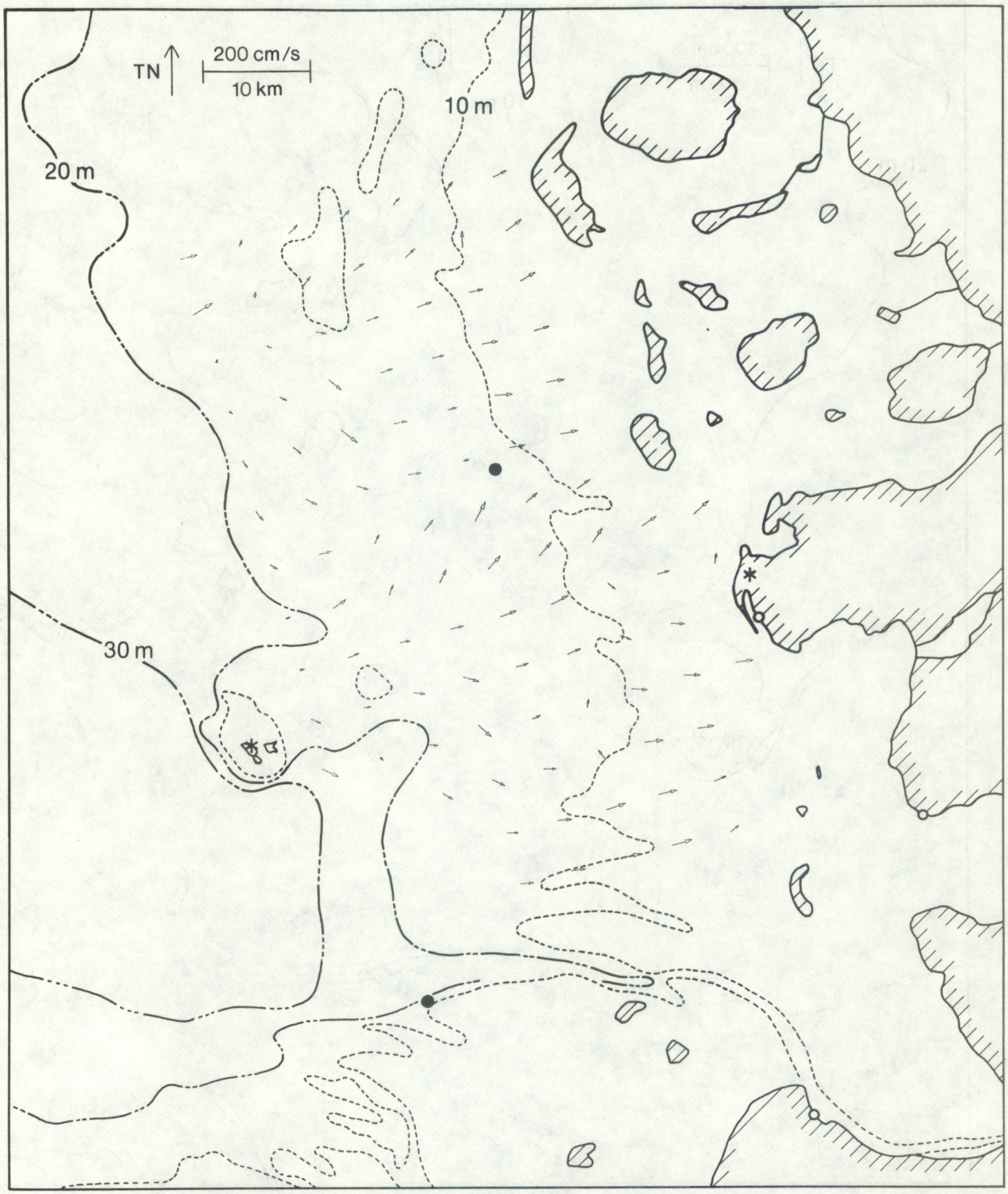

Figure 23.--Instantaneous surface current vectors 1200 21 September 1979.

Figure 24.--Instantaneous surface current vectors 1600 21 September 1979.

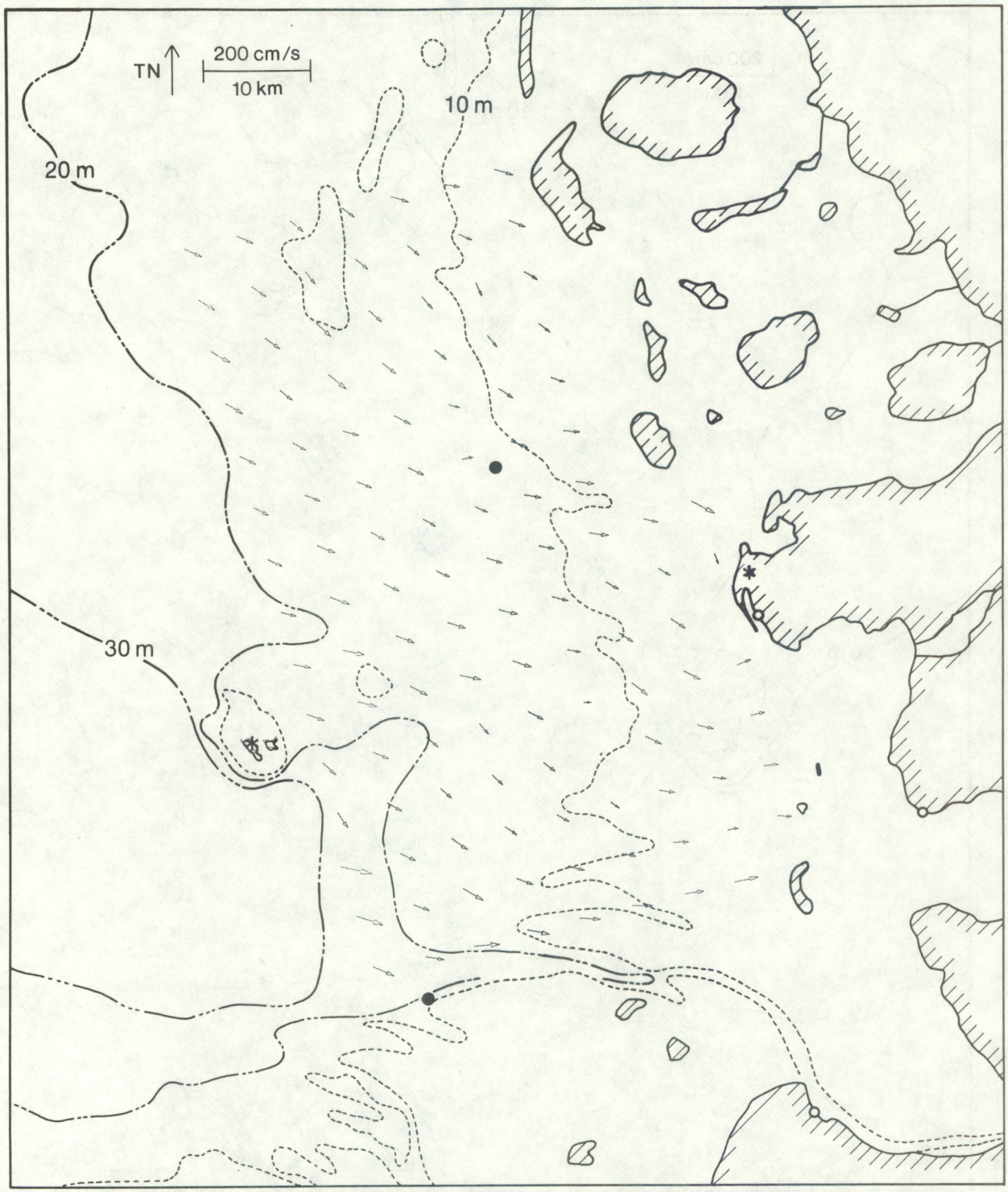

Figure 25.--Instantaneous surface current vectors 2000 21 September 1979.

Figure 26.--Instantaneous surface current vectors 0000 22 September 1979.

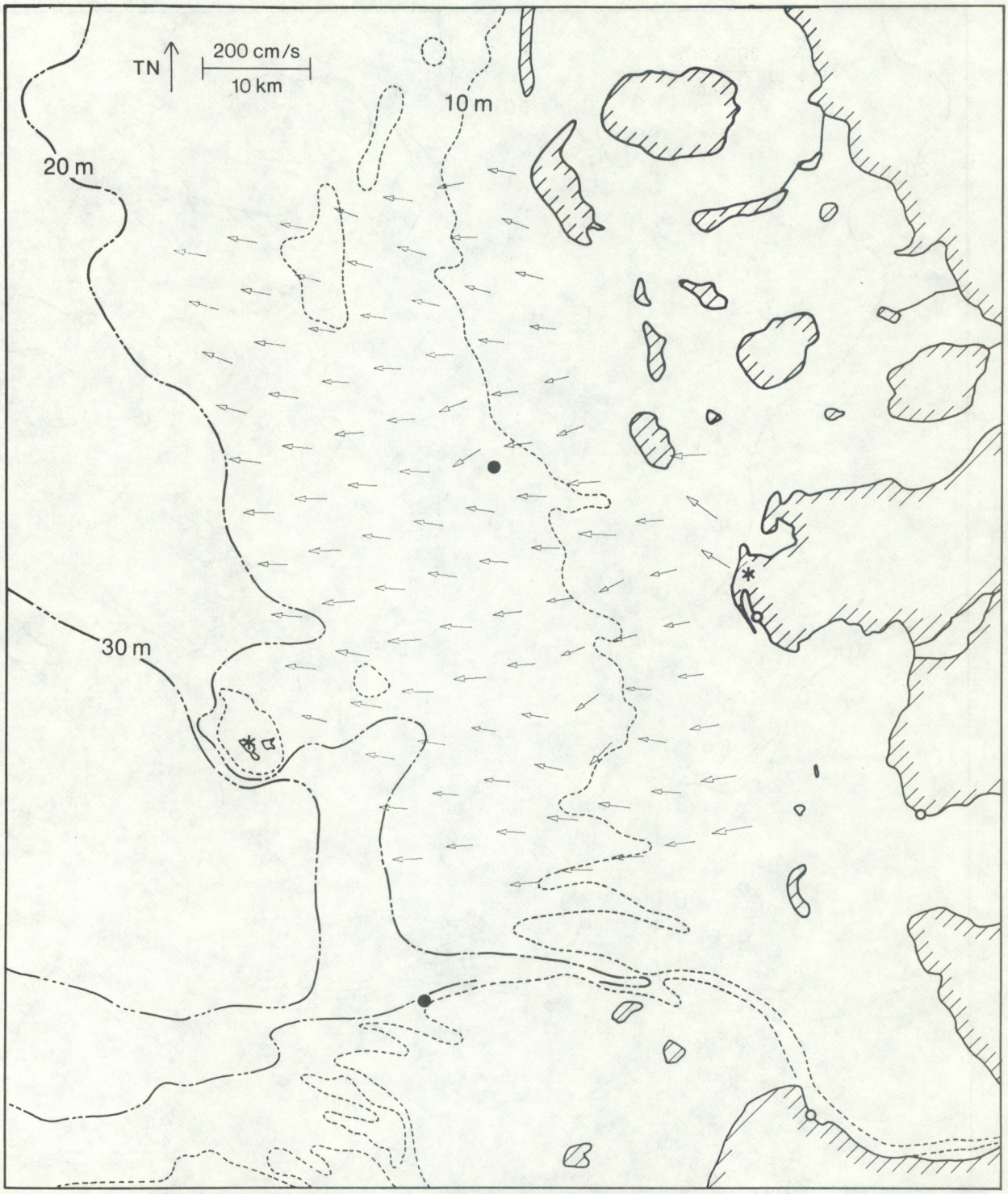

Figure 27.--Instantaneous surface current vectors 0400 22 September 1979.

Figure 28.--Instantaneous surface current vectors 0800 22 September 1979.

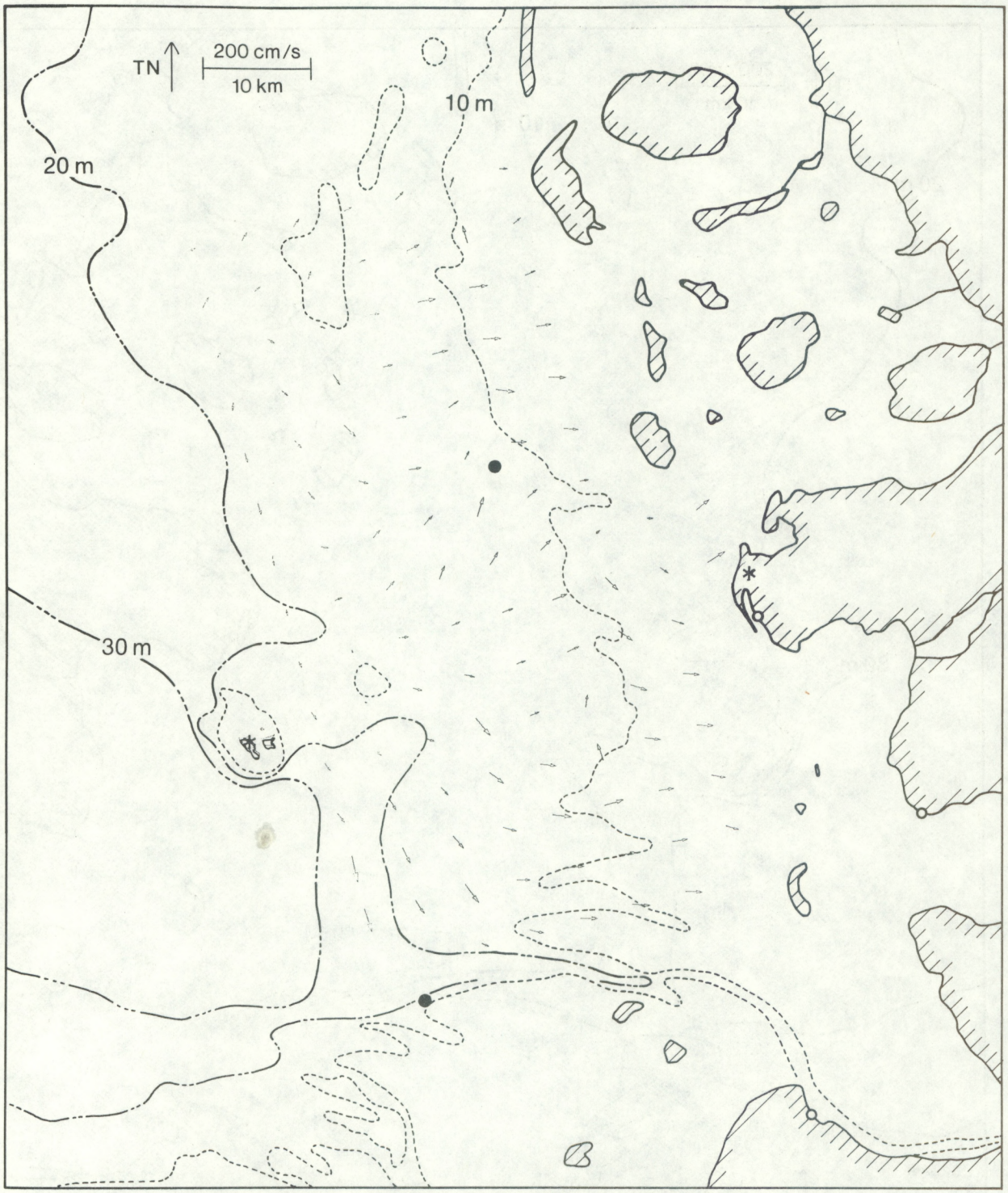

Figure 29.--Instantaneous surface current vectors 1200 22 September 1979.

Figure 30.--Instantaneous surface current vectors 1600 22 September 1979.

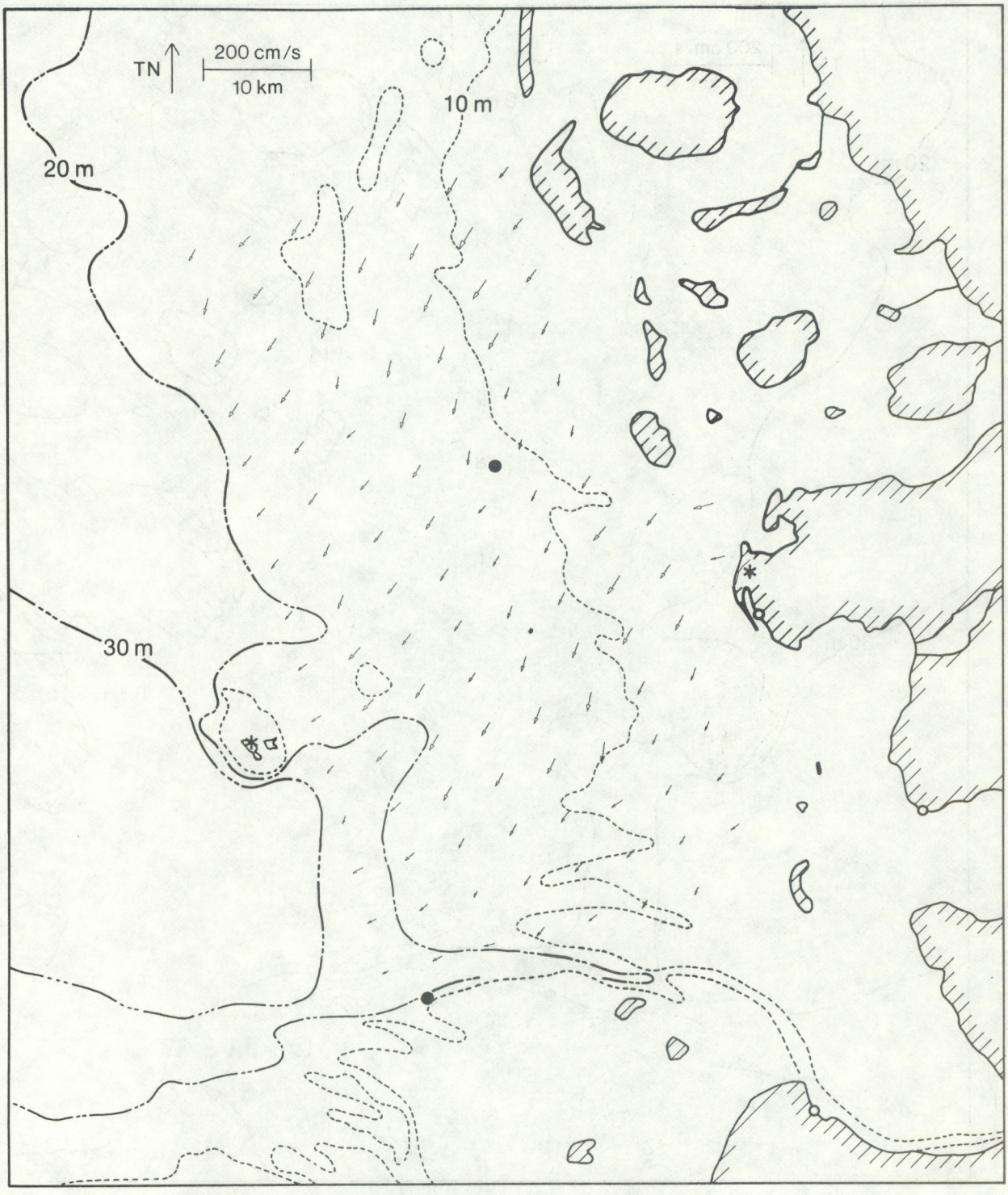

Figure 31.--Instantaneous surface current vectors 2000 22 September 1979.

Figure 32.--Instantaneous surface current vectors 0000 23 September 1979.

Figure 33.--Instantaneous surface current vectors 0400 23 September 1979.

Figure 34.--Instantaneous surface current vectors 0800 23 September 1979.

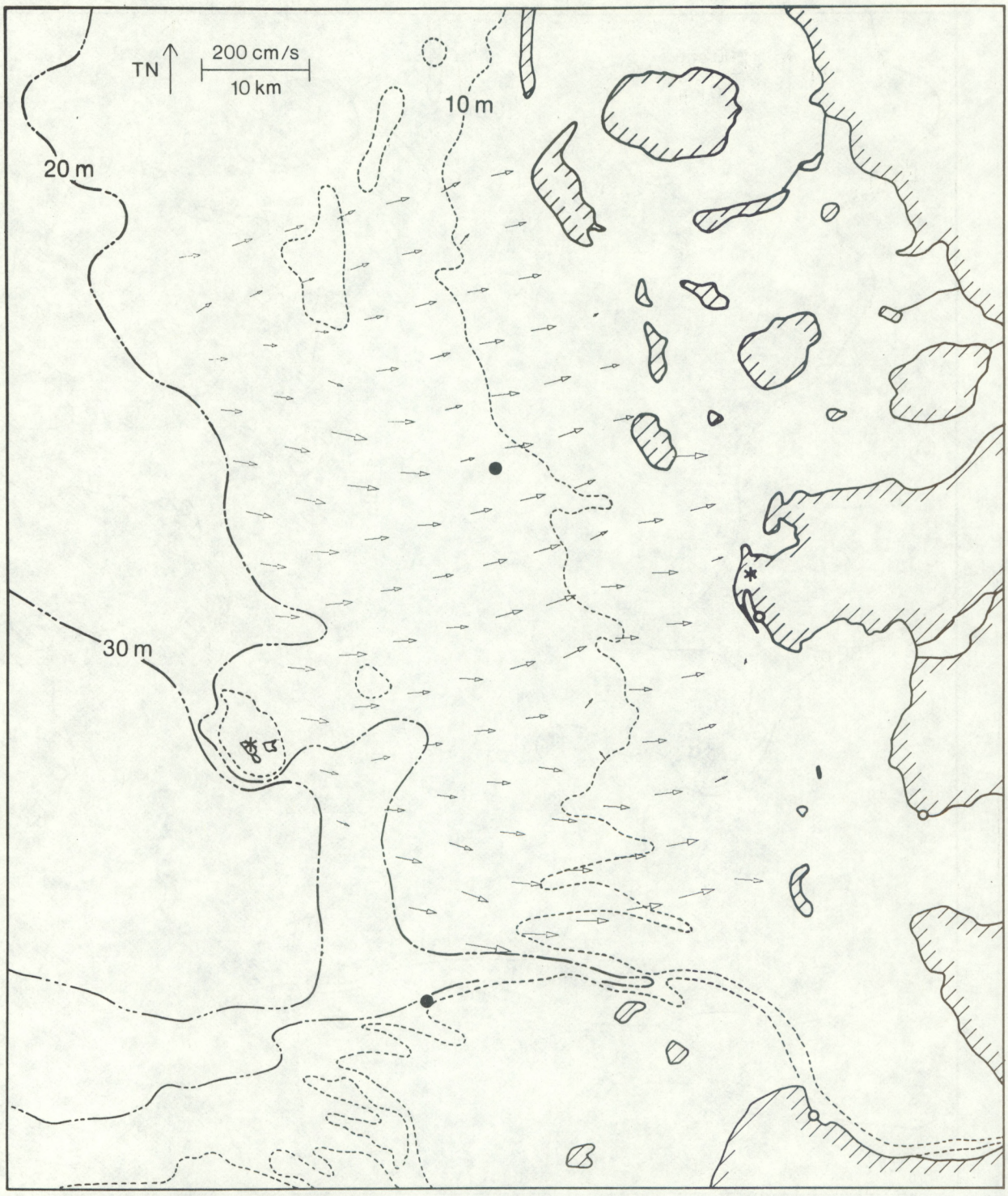

Figure 35.--Instantaneous surface current vectors 1200 23 September 1979.

Figure 36.--Instantaneous surface current vectors 1600 23 September 1979.

Figure 37.--Instantaneous surface current vectors 2000 23 September 1979.

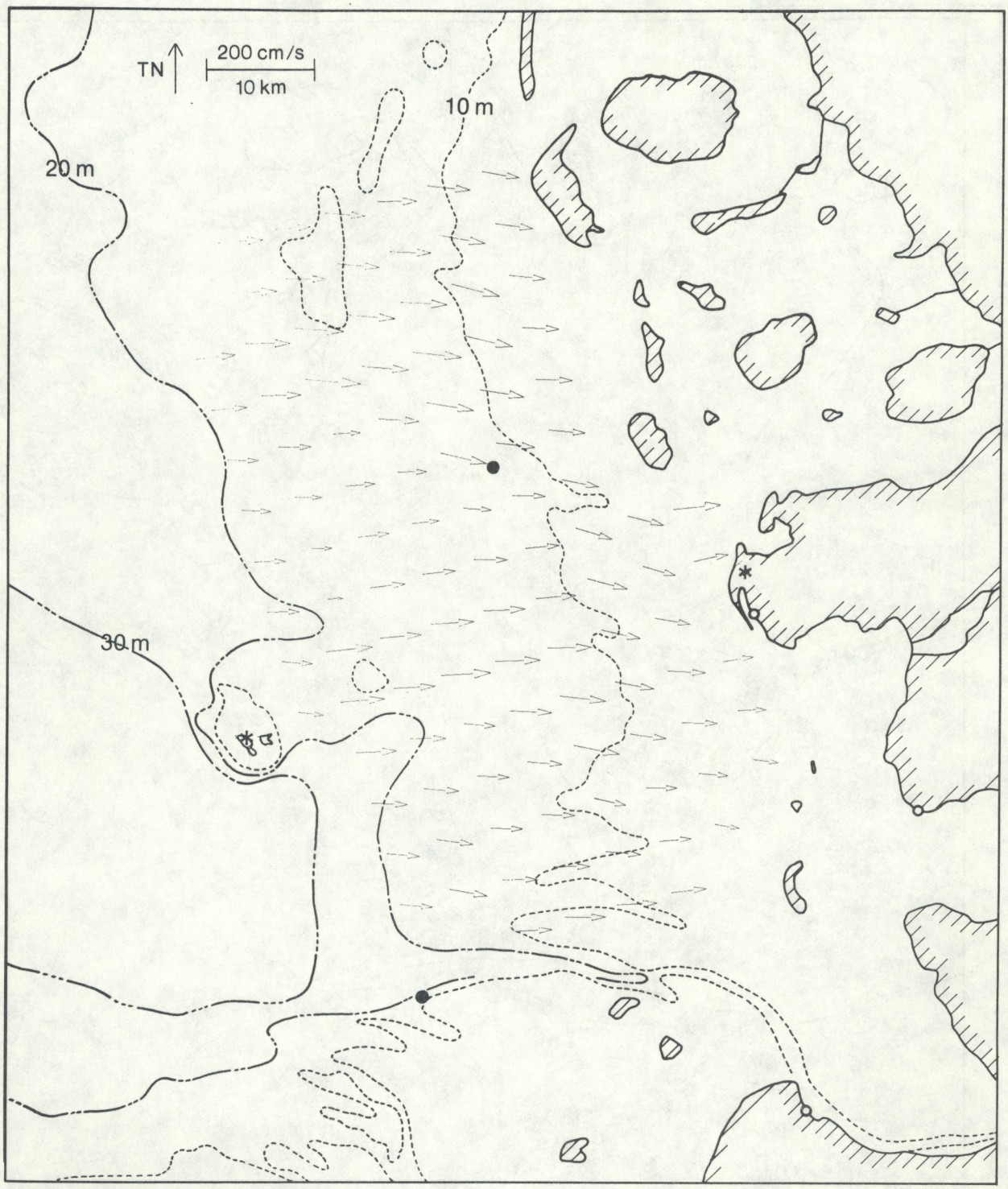

Figure 38.--Instantaneous surface current vectors 0000 24 September 1979.

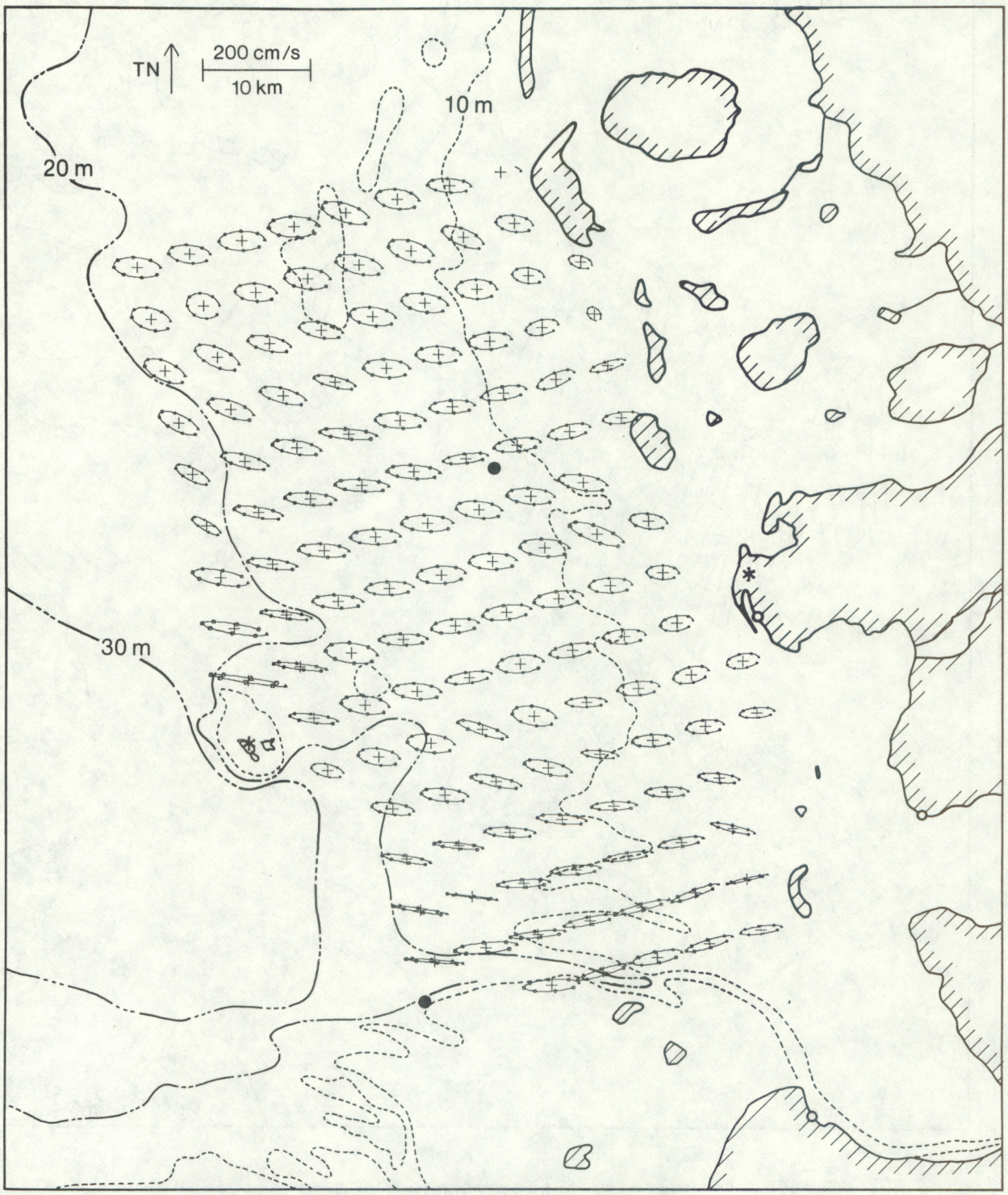

Figure 39.--Average semidiurnal tidal current ellipses 1722 17 September 1979 to 0036 24 September 1979.

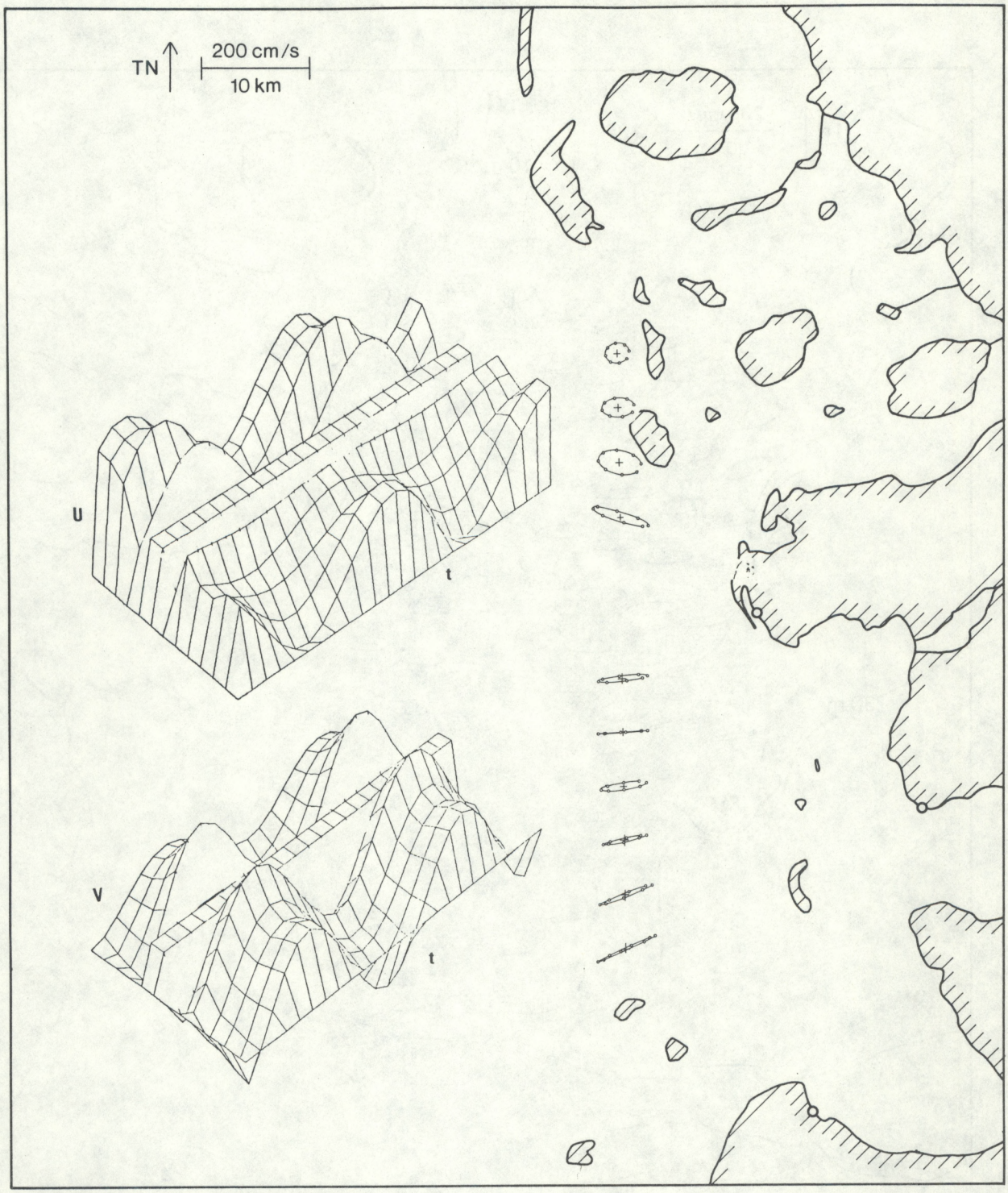

Figure 40.--Component analysis of the average semidiurnal tidal current ellipses approximately 12.5 km west of the coast 1722 17 September 1979 to 0036 24 September 1979. t is the time axis, each block is one of 24 hours. u is the component of velocity to the north, and v is the component of velocity to the west. Each line on the u and v axes represents one of the twelve ellipses. The scale of velocity for the ellipses does not apply to the graph.

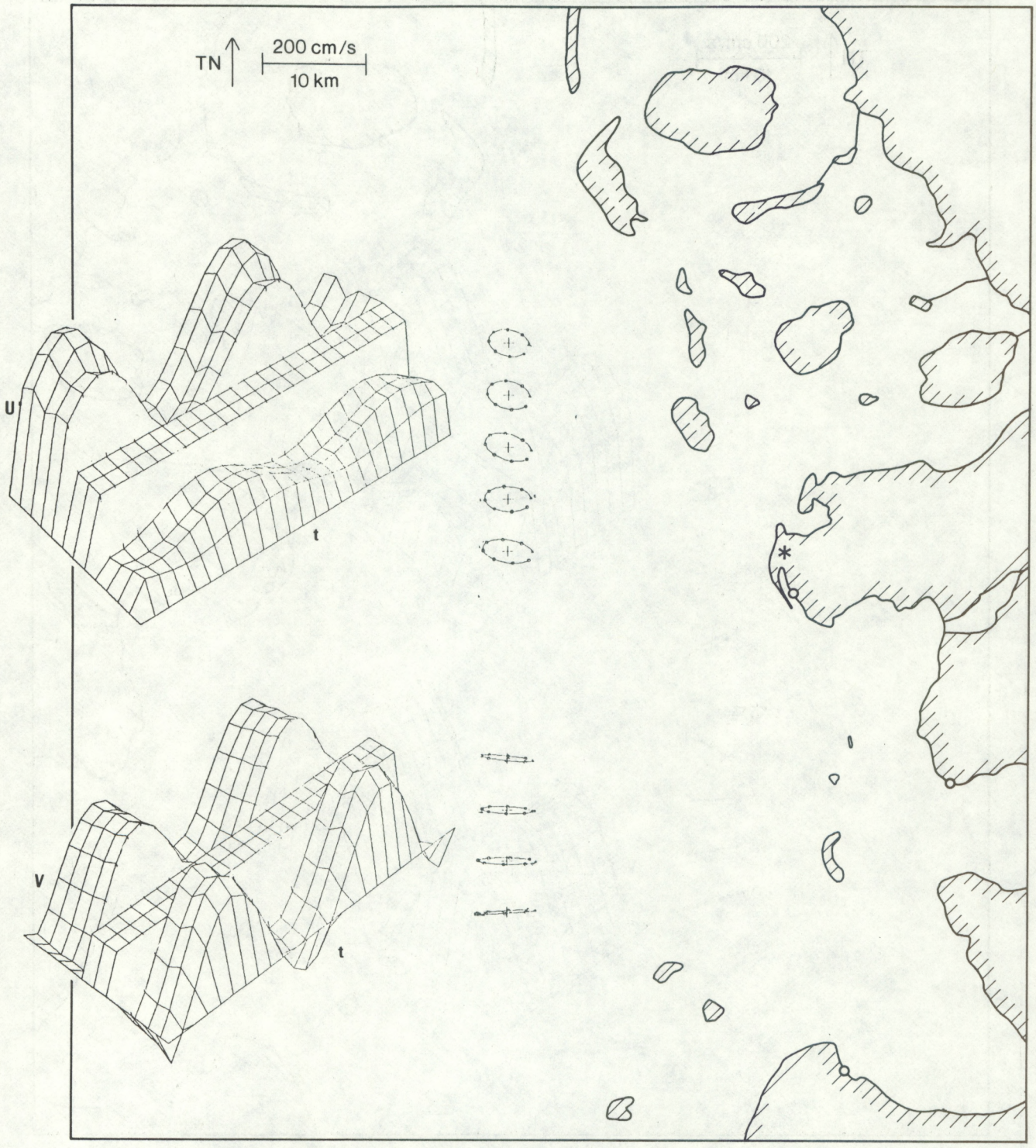

Figure 41.--Component analysis of the average semidiurnal tidal current ellipses approximately 27.5 km west of the coast 1722 17 September 1979 to 0036 24 September 1979. t is the time axis, each block is one of 24 hours. u is the component of velocity to the north, and v is the component of velocity to the west. Each line on the u and v axes represents one of the twelve ellipses. The scale of velocity for the ellipses does not apply to the graph.

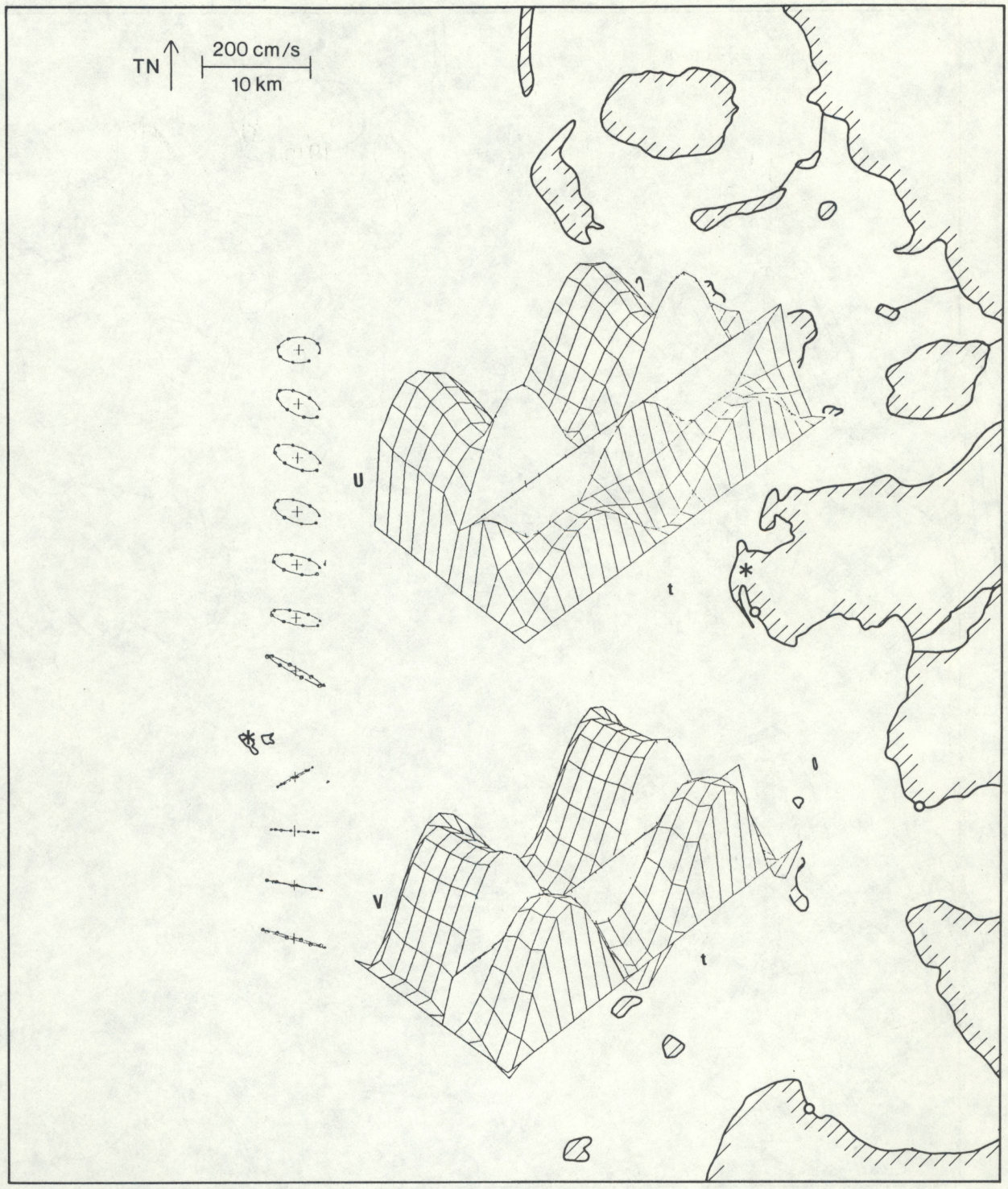

Figure 42.--Component analysis of the average semidiurnal tidal current ellipses approximately 42.5 km west of the coast 1722 17 September 1979 to 0036 24 September 1979. t is the time axis, each block is one of 24 hours. u is the component of velocity to the north, and v is the component of velocity to the west. Each line on the u and v axes represents one of the twelve ellipses. The scale of velocity for the ellipses does not apply to the graph.

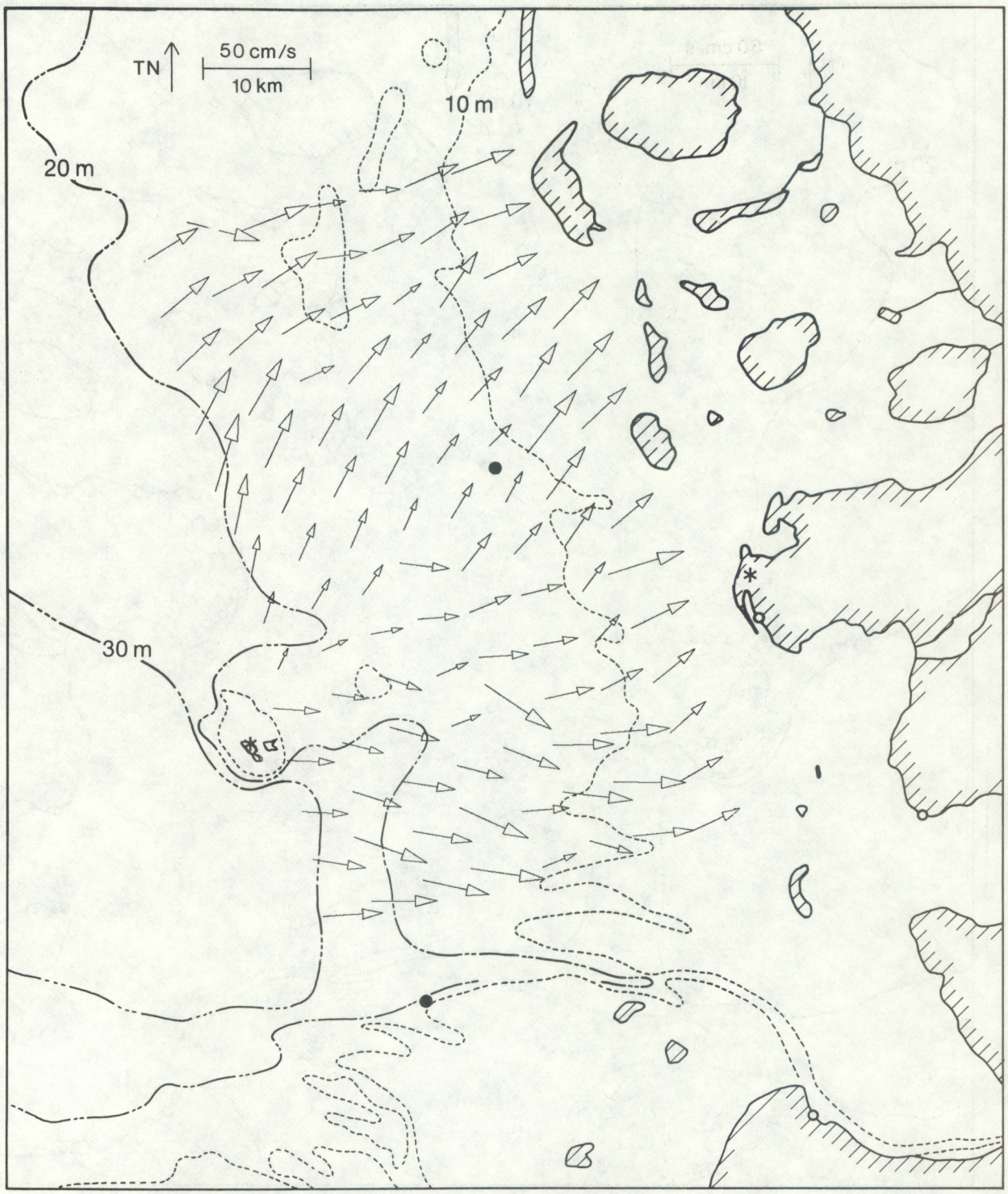

Figure 43.--Mean surface current vectors, semidiurnal tides removed, 0018 18 September 1979 to 0018 19 September 1979.

Figure 44.--Mean surface current vectors, semidiurnal tides removed, 0018 19 September 1979 to 0018 20 September 1979.

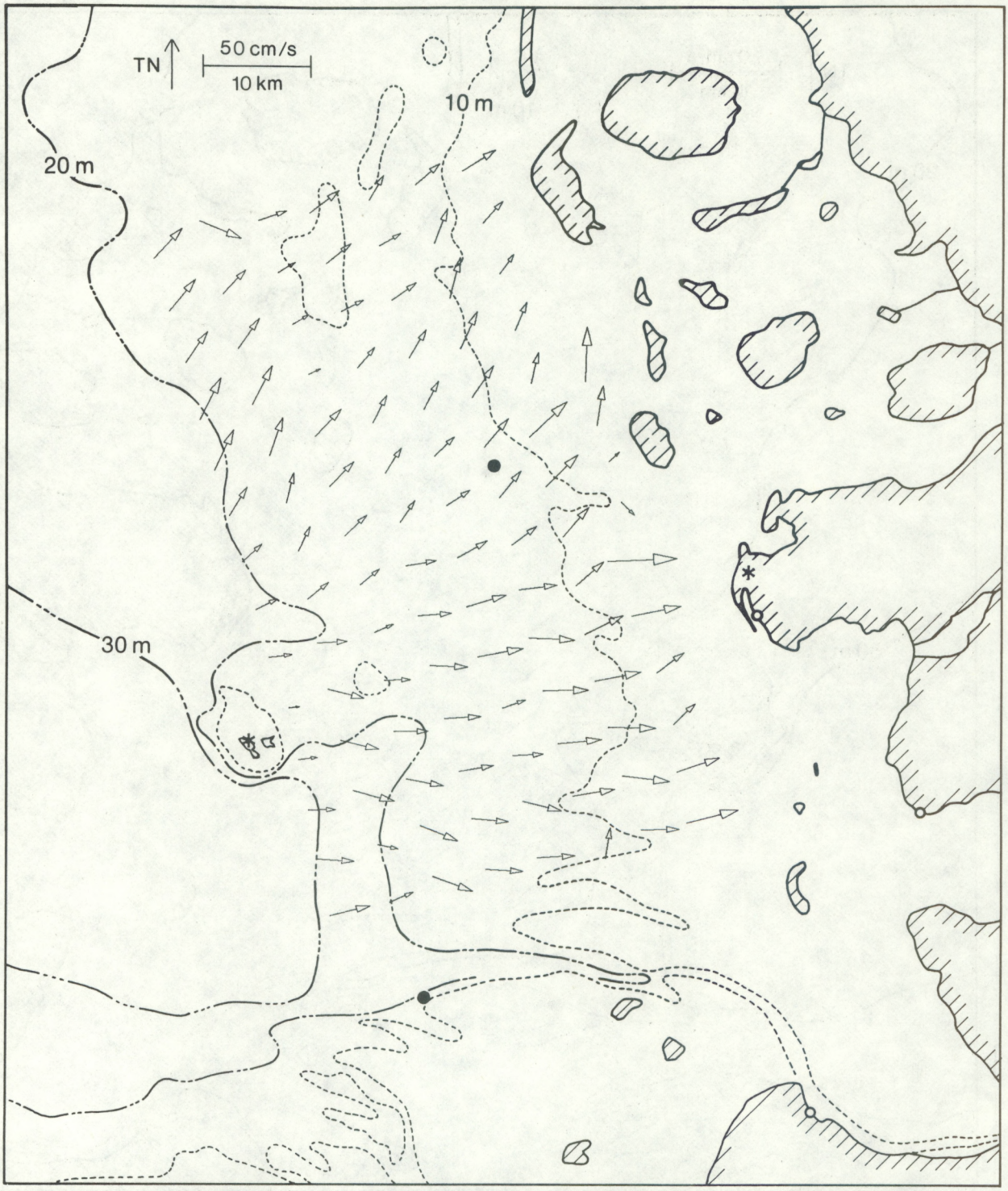

Figure 45.--Mean surface current vectors, semidiurnal tides removed, 0018 20 September 1979 to 0018 21 September 1979.

Figure 46.--Mean surface current vectors, semidiurnal tides removed, 0018 21 September 1979 to 0018 22 September 1979.

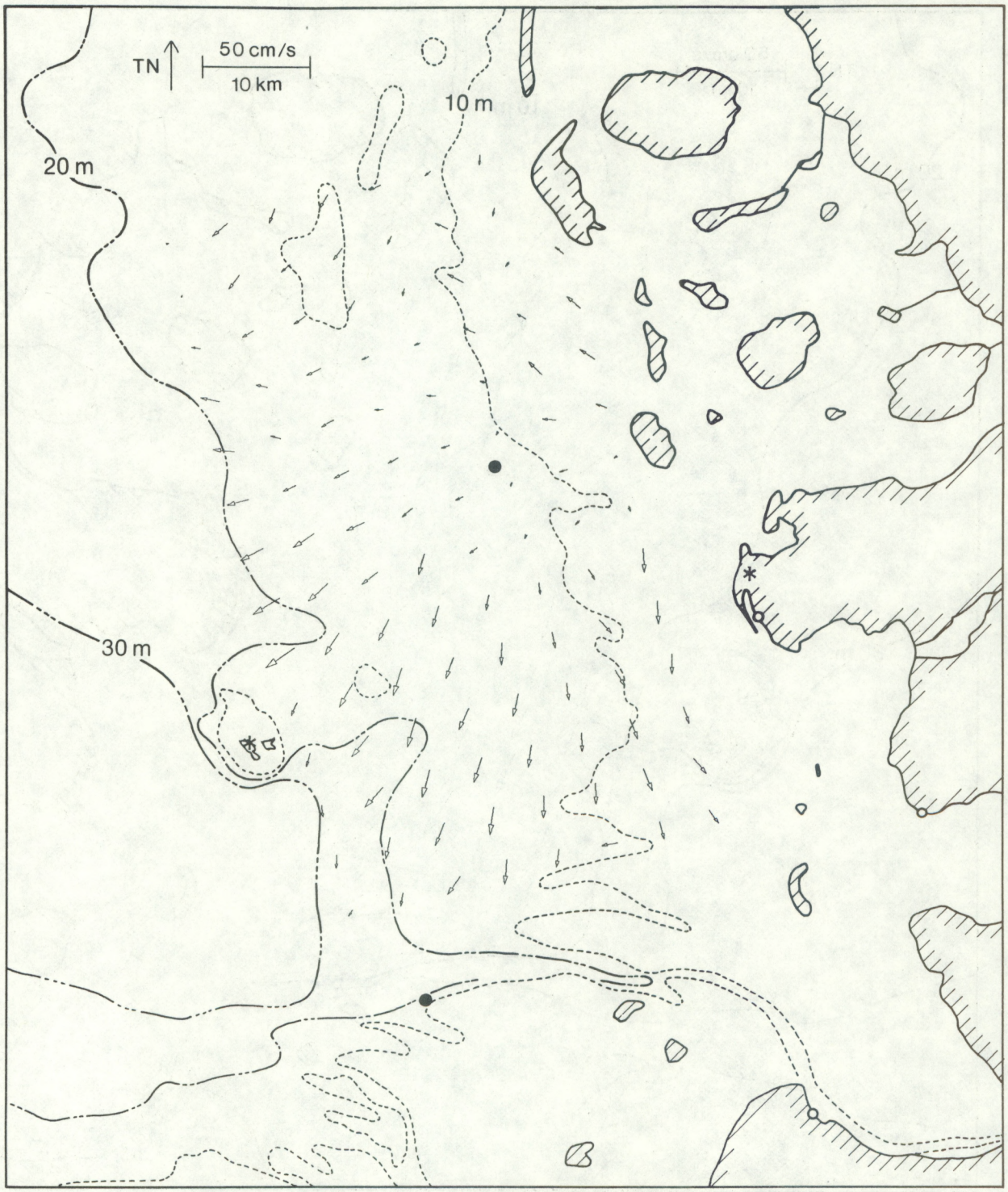

Figure 47.--Mean surface current vectors, semidiurnal tides removed, 0018 22 September 1979 to 23 September 1979.

Figure 48.--Mean surface current vectors, semidiurnal tides removed, 0018 23 September 1979 to 0018 24 September 1979.